



AN ABSTRACT OF THE THESIS OF

Justin B. Milliard for the degree of Master of Science in Geology presented on May 5, 2010

Title: TWO-STAGE OPENING OF THE NORTHWESTERN BASIN AND RANGE IN EASTERN OREGON: Evidence from the Miocene Crane Basin

Abstract approved:

---

Andrew J. Meigs

New data are presented that provide evidence for the onset of extensional deformation in the Northwestern Basin and Range within 1 million years after the eruption of the Steens Basalt at 16.5 Ma. New geologic mapping (1:24,000), stratigraphic sections, and  $^{40}\text{Ar}/^{39}\text{Ar}$  dating of the Crane Basin rocks provide a control of the structural and depositional history of the basin. Extension-related horst and graben formation began at 15.5 Ma and continued until  $\sim 7$  Ma. The Crane Basin, is one of a series of these half-grabens located to the east of the Harney Basin and Burns, Oregon on the footwall block of the Steens Mountain normal fault. Basin fill consists of volcanoclastic sedimentary rocks, tuffs, and lava flows. Key intra-basin marker beds include the 9.63 Ma Devine Canyon tuff and 11.5 Ma Visher Creek lava, in addition to a newly-discovered air fall ash with a  $\sim 12.5$  Ma age, the 7.25 Ma Drinkwater basalt, and the 1.93 Ma Voltage basalt age. Crane Basin strata unconformably onlap tilted Steens Basalt. Angular unconformities exist in the Crane Basin strata, between the basal sedimentary rocks, overlying Devine Canyon tuff and capping Drinkwater basalt. Fault histories in the Crane Basin record similar rates

of displacement from ~15.5 Ma to 9.63 Ma, divergent and heightened rates from 9.63 to 7.25 Ma and extremely slow rates after 7.25Ma. Together, these observations indicate that broad extensional deformation initiated following the eruption of the 16.5 Ma Steens Basalt and continuing until ~9.63 Ma (STAGE 1). After ~9.63 Ma deformation became heterogeneous and localized, migrating east to west, eventually shifting from the Crane Basin to the Harney Basin. The field relationships signal that the second deformational event was short-lived, ceased by ~7Ma (STAGE 2). Post 7.25 Ma the displacement on Crane Basin faults and the Harney Basin depositional record demonstrates that only minor fault deformation occurred. The findings of this study provide a previously undocumented resolution of the development stages of the margin of a continental extensional province. Moreover, these new data demonstrate a “temporal” link between magmatic and tectonic activity in Southeastern Oregon, suggesting that both deformation mechanisms jointly accommodated extensional strain at the margin of the developing Basin and Range Province.

© Copyright by Justin B. Milliard

May 5, 2010

All Rights Reserved

TWO-STAGE OPENING OF THE NORTHWESTERN BASIN AND RANGE IN EASTERN  
OREGON: Evidence from the Miocene Crane Basin

by

Justin B. Milliard

A THESIS

Submitted to

Oregon State University

in partial fulfillment of  
the requirements for the  
degree of

Master of Science

Presented May 5, 2010

Commencement June 2010

Master of Science thesis of Justin B. Milliard presented on May 5, 2010.

APPROVED:

---

Major Professor, representing Geology

---

Chair of the Department of Geosciences

---

Dean of the Graduate School

I understand that my thesis will become part of the permanent collection of Oregon State University libraries. My signature below authorizes release of my thesis to any reader upon request.

---

Justin B. Milliard, Author

## ACKNOWLEDGMENTS

There are far too many people in my life who have contributed to my effort in the past three years to thank but here it goes. Foremost, I would like to thank my advisor, Professor Andrew Meigs, first for giving me the opportunity to do this and for his guidance and support, second for kicking me in the butt when needed, and lastly for *not* kicking me out the door when many others might have. Secondly, my committee members Anita Grunder and John Dilles whose advice and guidance I have benefited greatly from and whose patience has allowed me to reach this point.

I would also like to thank the members of my family and my small circle of friends (I don't want to make you jealous of one another, so I'm not naming names). All of you gave me the reassurance to see this project through from beginning to end, and while you may not have understood Crane geology you understood its frustrations.

Along with learning a thing or two about geology through this project, I also had the opportunity to get to know the people of eastern Oregon. As one of my colleagues said, "They are the true salt of the earth". I could not phrase it better. Along with being given a roof over my head, a bed to sleep in, and a table and a family to share dinner with, the Miller family gave me a second home, at their ranch and in the Crane community.

I also want to thank the numerous people who have aided me during my geologic journey: Marc Hendrix, Jim Sears, and Don Winston at the University of Montana, all of whom nurtured my love for the science and pushed me further than I would voluntarily have gone. Mike Satre, at the Greens Creek Mine in Alaska, who provided me with an invaluable experience and said, "Beer, fishing & skiing, is there more to life?" Joe Watson at Pason Systems USA for paying me to work on the Colorado Plateau and teaching me the importance geology plays in today's

world. To quote, "If you can't grow it, you must drill or mine it!". Jim Moum at OSU, the COAS Ocean Mixing Group, and Ren-Chieh Lien of the University of Washington APL, who gave me the opportunity to try my hand at conducting physical oceanography research.

Thank you to the entire faculty, staff and my fellow students at Oregon State University, who have now put up with me for 3+ years.



## CONTRIBUTION OF AUTHORS

During the course of my study I have had the privilege to discuss, talk and argue with numerous people about the geology of eastern Oregon. Andrew Meigs, Anita Grunder, John Dilles, Mark Ford, Kaleb Scarberry, Ajeet Johnson, Alex Ramsey and others have helped me shape my ideas of the Crane Basin and the Northwestern Basin and Range.

## TABLE OF CONTENTS

	<u>Page</u>
Introduction.....	1
Geologic Setting.....	3
Problem Statement.....	6
Methods.....	8
Regional Stratigraphy.....	8
Cross-Sections.....	23
Methods.....	23
Local Structural Framework.....	28
Scissor-type Normal Faults.....	29
Results.....	30
Total Extension.....	30
Fault History.....	31
Stratigraphic Constraints on the Onset of Extension.....	31
Timing of Extension.....	32
Onset.....	32
Eastern Crane Basin.....	33
Western Crane Basin.....	33
2-Stage Deformation.....	34
Crane Basin Evolution.....	34
Harney Basin Evolution.....	36
Results.....	40
Conclusion.....	42
Crane School District Field Trip.....	48
Bibliography.....	50
Appendix.....	57

## LIST OF FIGURES

<u>Figure</u>	<u>Page</u>
1: Tectonic Setting of Crane Basin study area.....	2
2: Map of southeastern Oregon and extensional basins.....	5
3: Map of the Crane and Harney Basins.....	7
4: Geologic Map of the Crane Basin.....	10
5: $^{40}\text{Ar}/^{39}\text{Ar}$ age plateaus .....	14
6: Partial cross sections	
A) Structural relationships of the Eastern Crane Basin.....	16
B) Structural relationships of the Western Crane Basin.....	17
7: Spiderplot comparison of Crane Basin tuffs.....	21
8: Crane Basin cross sections.....	24
9: Domino-style fault block model	
A) Crane Basin schematic example.....	26
B) Half-graben filling model.....	26
10: Annotated picture of exposed Western Crane Basin half-graben.....	26
11: Two-Stage Crane Basin fault record	
A) Horizontal displacement rate.....	35
B) Separation history.....	35
12: Harney Basin evacuation history	
A) Map of Harney Basin base levels.....	39
B) Topographic profiles of intra-basin lava flows.....	40
13: Map of the Northwestern margin of the Basin and Range cataloguing both structural and volcanic events of its development.....	45
14: Crane Basin School District field trip.....	49

LIST OF TABLES

<u>Table</u>	<u>Page</u>
1: Harney Basin exploration wells.....	38

LIST OF EQUATIONS

<u>Equation</u>	<u>Page</u>
1: Horizontal extension calculation adapted from Wernicke (1982).....	27

LIST OF APPENDICES

<u>Appendix</u>	<u>Page</u>
AF1: Stratigraphic Section location map and Key.....	58
AF2: Stratigraphic Section 1.....	59
AF3: Stratigraphic Section 2.....	63
AF4: Stratigraphic Section 3.....	64
AF5: Stratigraphic Section 4.....	64
AF6: Stratigraphic Section 5.....	65
AF7: Stratigraphic Section 6.....	66
AF8: Stratigraphic Section 7.....	67
<sup>40</sup> Ar/ <sup>39</sup> Ar Dating	
Methods.....	68
Results.....	69
Table 1: Summary Table of <sup>40</sup> Ar/ <sup>39</sup> Ar.....	71
XRF and ICP-MS Geochemistry	
Methods.....	72
Results.....	73
Table 2: Summary Table of ICP-MS analyses.....	74
Table 3: Summary Table of XRF analyses.....	75
Table 4: Summary Table for geochemical data used in Figure 7 spiderplot.....	77
Table 5: Summary Table for <sup>40</sup> Ar/ <sup>39</sup> Ar analysis of Voltage basalt.....	78
Table 6: Summary Table for <sup>40</sup> Ar/ <sup>39</sup> Ar analysis of Swamp Creek ash.....	79
Table 7: Summary Table for <sup>40</sup> Ar/ <sup>39</sup> Ar analysis of Drinkwater basalt.....	80
Table 8: Summary Table for <sup>40</sup> Ar/ <sup>39</sup> Ar analysis of Swamp Creek ash.....	81

## LIST OF PLATES

Plate

1. Geologic Map of the Crane Basin
2. Cross Sections of the Crane Basin

Plates are located in the pocket at the back of the book.

## **Introduction**

To understand the stresses and processes responsible for the development and migration of the Northwestern Basin and Range (NWBR), a thorough understanding of the map distribution, structure, and stratigraphic relationships of the eastern Oregon volcanic rocks must be attained (Camp, 2003). Extensional basins provide perhaps the most important record of the history of the stretching of the Earth's crust, because they contain structures that were active during sedimentation and commonly have strata that provide the necessary chronologic constraints for dating the structures (Schlishe, 1994).

A complex and well-developed mid to late-Miocene extensional fault fabric characterizes the northwest margin of the Basin and Range east of Burns, OR (Figure 1). The fabric is dominated by north-south striking moderate displacement (>100m) normal faults as well as synthetic, and antithetic normal faults with minor displacement (<100m). Moderate displacement faults form a series of domino-style blocks whose subsidence formed a series of half-graben depocenters. The collective basin formed by the depocenters has been termed the Crane Basin and is the focus of this study. Deposition of sediment was localized along the axial fault traces of the down-thrown hanging wall blocks. The strata visibly thicken toward the fault trace (westward) and thin away from the fault (eastward), where units' onlap the bedrock units of Steens Basalt and rhyodacite. Volcaniclastic strata filling the half-graben represent a continual record of deposition from ~15.5 Ma to 7 Ma. Dated key marker beds provide a high resolution chronological record that constrains both subsidence and fault rates.

Utilizing the complete Crane Basin stratigraphic record to understand the structural evolution of the Crane Basin region this study aims to document the developmental stages of the northwestward margin of the Basin and Range. Previous research conducted on the northwestern margin of the Basin and Range suggests that its westward progression occurs in epi-

sodic, heightened stages of activity (Meigs, 2009; Trench, 2008), but limitations in the geologic record have failed to allow tight constraint on the timing of events. The goals of this project

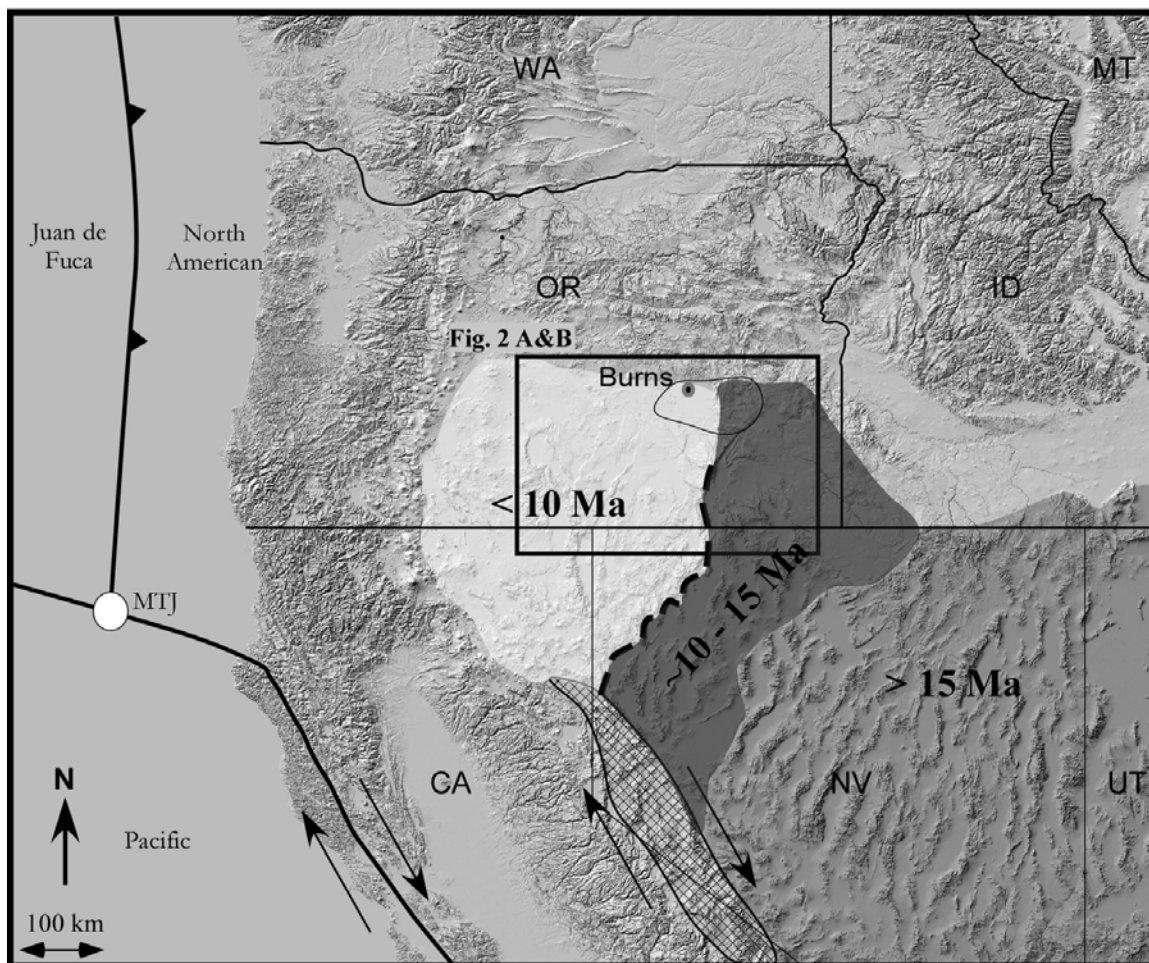


Figure 1. Shaded relief map of the northwestern United States. Continental plate boundaries are shown. Between the North American Plate and the Juan de Fuca is the Cascadia Subduction Zone and between the North American Plate and the Pacific Plate is the Sand Andreas Fault and related Walker Lane (cross-hatched region). The >15 Ma well developed fabric of the Basin and Range, characterized by distinct parallel ranges and valley is shaded medium gray. The 10-15 Ma transition zone is shaded dark gray, and the <10Ma poorly developed Basin and Range fabric is shaded white. (Basin and Range age regions adapted from Colgan (2006). A distinct structural boundary separates the well developed structural fabric >10Ma from the poorly developed fabric <10Ma (highlighted by thick dashed line). Location of the Crane and Harney Basin depocenters study area are outlined by thin line around the town of Burns, OR. Notice location of study area uniquely lies on the northern margin of the Basin and Range and straddles the transitional and younger Basin and Range domains. [MTJ: Mendocino Triple Junction; CA: California; ID: Idaho; MT: Montana; NV: Nevada ; OR: Oregon; WA: Washington]. Inset black rectangle outlines the area of Figure 2.



were to catalogue the highest resolution geologic record of the development of the margin of the Basin and Range. Addressing the questions of “when” the northwestern structural boundary of the Basin and Range formed and “how” it evolved in space and time, from the immature stage of an un-faulted plateau to the mature stage of distinct horst and grabens. Research for this project focused on 1:24,000 scale field mapping of a 50 square kilometer area adjacent to the town of Crane, OR. This field area encompasses a portion of the mid-Miocene age Crane Basin and overlaps with the late-Miocene to Pliocene age Harney Basin. This overlap allowed research to utilize the stratigraphic record of both basins to create a well constrained timeline of structural development.

## **Geologic Setting**

The Northwestern Basin and Range refers to the NW part of the Basin and Range Province in southeastern Oregon. This region is dominated by mid to late-Cenozoic volcanic rocks that have been erupted upon a basement of Mesozoic and older accreted terranes juxtaposed to the North American craton (Camp, 2003; Vallier, 1995). The NW part of the Basin and Range Province describes a region of gently tilted normal-fault blocks, understood as the result of lithospheric extension in the backarc of the Cascade arc, and contiguous with the Basin and Range of Nevada – Utah to the southeast (Christiansen, 1992). Back arc extension accompanied clockwise rotation of the Cascades-Coast Range-Klamath Mountains to the west of the arc (Christiansen, 1992). To the east of the arc extensional faulting in Nevada was active between 45 Ma - present (Christiansen, 1992; Colgan, 2006; Dickinson, 2002; Lerch, 2008; Meigs, 2009; Scarberry, 2009). The extent of the Basin and Range Province has migrated from central Nevada, where it initiated, and northwestwards into southeastern Oregon during the past 15 Myr (Meigs, 2009; Scarberry, 2009; Trench, 2008).

A structural boundary runs from the Steens Mountain fault in Oregon at its NE limit to the NW tip of the Walker Lane in California at its SW limit. The boundary separates a region of >15 Ma well developed extension terrain in the central Basin and Range from a <10 Ma domain in the NW corner of the Basin and Range. This younger structural fabric to the west of the boundary formed the Winter Ridge, Abert Rim, Poker Jim Rim, and Catlow Rim (Scarberry, 2009) (Figure 2). The Steens Mountain fault strikes north-northeast from the Pueblo Mountains along the Oregon–Nevada border to Turnbull Mountain where its topographic expression diminishes to zero. A closer investigation of this region suggests that the crust has not yet experienced significant extension to develop organized, reactivated faults (Anderson, 1983; Wallace, 1979) and is the youngest manifestation of the northwestward migration of Basin and Range tectonics. North of Turnbull Mountain recent studies by Cummings (2000) on the Oregon-Idaho Graben (OIG), a northeast trending synvolcanic graben that formed from 15.5 Ma to 10.5 Ma, suggest a distributed deformational front migrated north from the tip of the Steens Mountain fault.

West of the Oregon-Idaho Graben, a north-south trending normal fault network developed contemporaneously and preceded multiple half-graben depocenters that formed the greater Crane Basin. Deposition across the greater basin occurred primarily from ~15.5 Ma – 9.63 Ma, when fault development fundamentally changed, limiting deposition to localized half-grabens that accumulated sediment up to ~7 Ma. 100km far to the north in the John Day Valley, a large east-to-west trending normal fault bounded half-graben valley appears to have also formed during this time period. Its formation is recorded by displaced 16.1 Ma Picture Gorge basalts (Baksi, 1989) and largely undeformed 7.05 Ma Rattlesnake ash-flow tuff (Streck, 1995) capping the valley fill. The Grasshopper Flat and Harney Basin lie to the north and west of the Crane Basin exists, respectively. The Grasshopper Flat is a late-Miocene age, northwest trend-

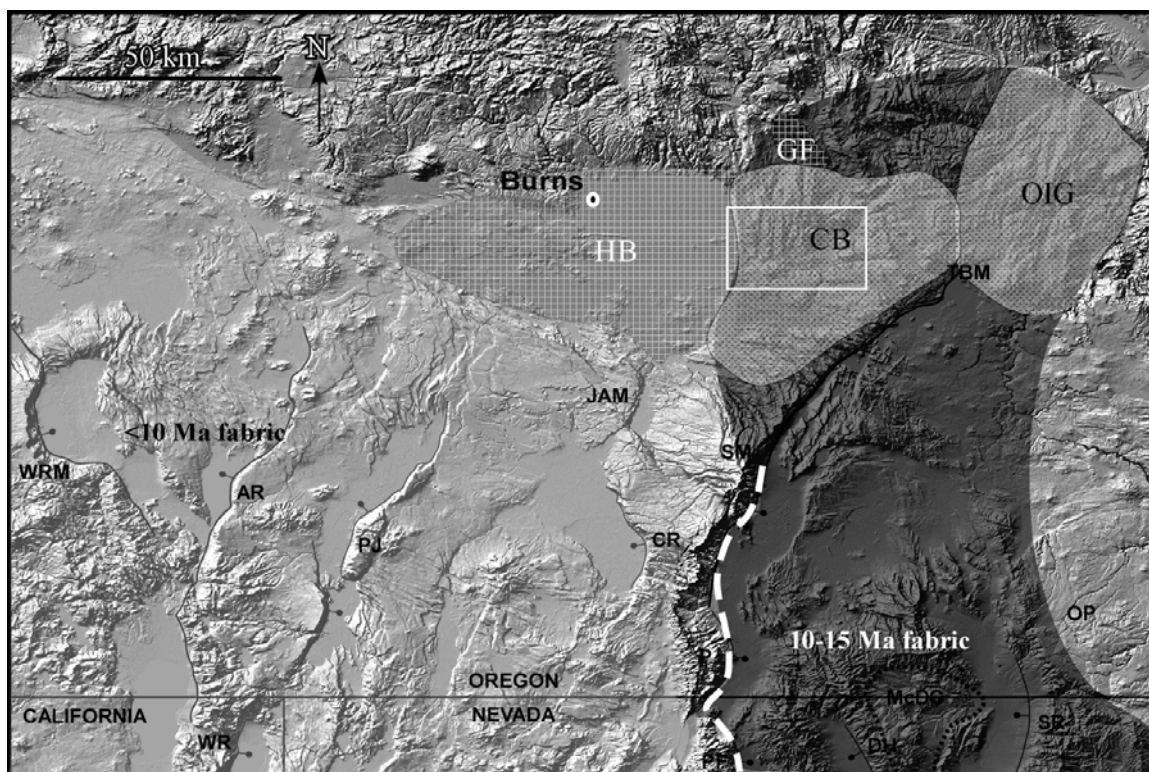


Figure 2. Shaded relief map of southeastern Oregon illustrating the topography which is controlled by extensional structures at the northern margin of the Basin and Range. The white dashed-line marks the structural boundary between the transitional (dark gray) and young (white) domains of the Basin and Range. At the northern margin of the Basin and Range are four Miocene age, extensional basin depocenters [CB: Crane Basin; GF: Grasshopper Flats; HB: Harney Basin; OIG: Oregon-Idaho Graben]. The white rectangle defines the study area and geologic map (Figure 4). [AR: Abert Rim; CR: Catlow Rim; DH: Double H Mountains; JAM: Jackass Mountain; McD: McDermitt caldera; PF: Pine Forest Range; PJ: Poker Jim Rim; SM: Steens Mountain; OP: Owyhee Plateau; SR: Santa Rose range; SV: Surprise Valley fault; TBM: Turnbull Mountain; WM: Warner Rim; WRM: Winter Ridge]

ing, fault accommodated, down-warping synform depocenter (Johnson, 1998). The Harney Basin is a late-Miocene age depocenter that is a regional geologic anomaly due to its unusually large dimensions and poorly understood formation.

During the late-Cenozoic in southeast Oregon volcanic activity occurred contemporaneously with crustal extension. Volcanic rocks of the southeastern Oregon region can be distributed into two temporal and compositional groups, an older 16.6 Ma to 15.3 Ma tholeiitic mafic

to bimodal assemblages related to the Steens Mountain flood basalts (Camp, 2003) and younger ~12 Ma to the present high-alumina olivine tholeiites to calc-alkaline mafics and rhyolites of the High Lava Plains (HLP) (Carlson, 1987, 1988; Jordan, 2002; Jordan, 2004). The HLP province forms an elongate trend east to west across the northern margin of the Basin and Range. Silicic volcanism of the HLP, displays a westward younging-age progression (Figure 3). At the eastern end of the HLP, three voluminous plinian-style eruptions occurred from with the Harney Basin, the 9.63 Ma Devine Canyon tuff (>300km<sup>3</sup>), the 8.41 Ma Prater Creek tuff (~200km<sup>3</sup>), and the 7.05 Ma Rattlesnake tuff (>300km<sup>3</sup>) (Christiansen, 1992; Jordan, 2004; Streck, 1999a, b). Mafic volcanism is not age-progressive, but was punctuated by large volume events at approximately 7.6 Ma , 5.9 Ma, 2-3 Ma respectively (Jordan, 2004). The 7.6 Ma episode was the most volumetrically significant.

## **Problem Statement**

As the structure of Basin and Range extension evolves from the initial immature stages as seen in the Oregon Plateau to the mature stages of well developed N-S oriented horst and grabens as in central Nevada, the structural fabric becomes more organized. Broad regions of dispersed faults and sub-basins coalesce to form a mature, simplified basin geometry (Anderson, 1983). Examples of the initial stages of Basin and Range development on its NW margin have yet to be adequately documented due to lack temporal resolution in the geologic record.

Immediately west of the Steens Mountain fault exist a series of moderate offset (>100m) normal faults that formed a Miocene age extensional basin depocenter, the Crane Basin. The Crane and neighboring Harney Basin preserves a continuous stratigraphic record ranging from prior to extension at 16.5 Ma to present day. This geologic record records the devel-

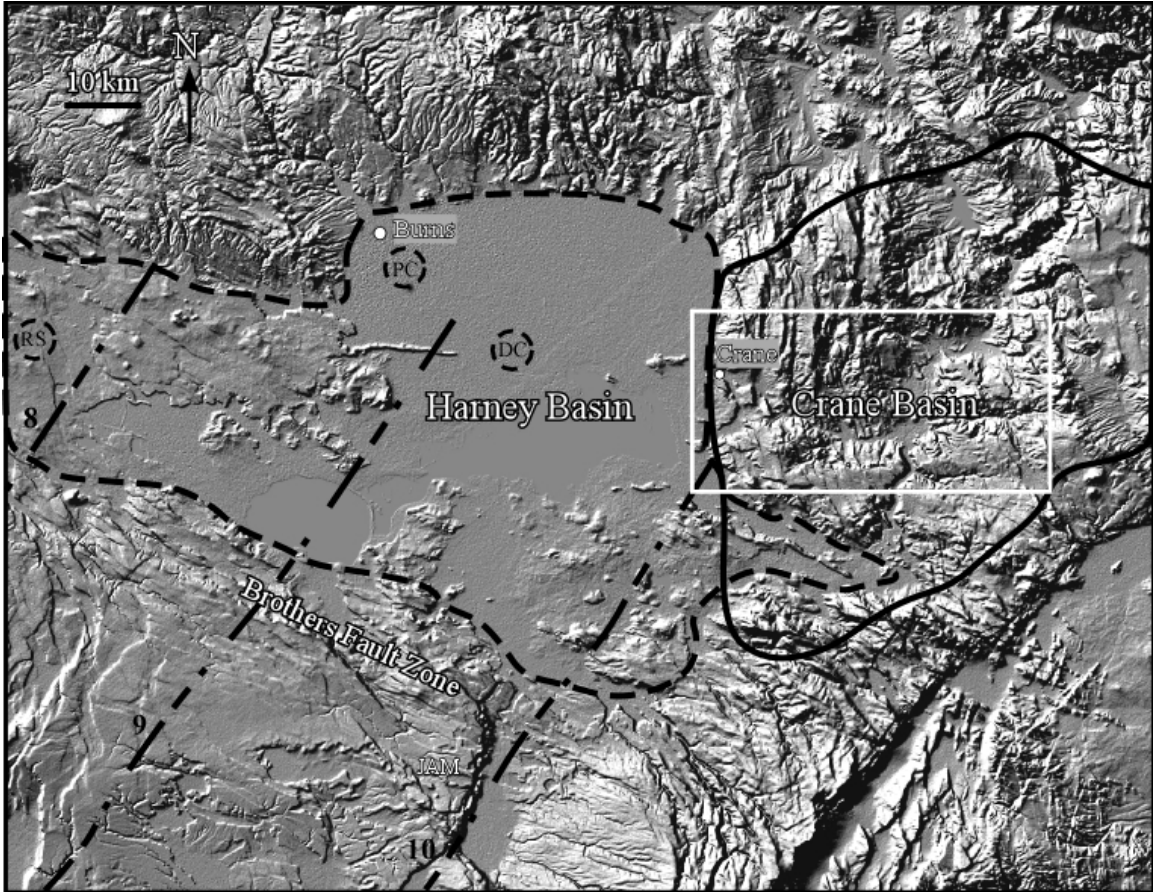


Figure 3. DEM of region surrounding the study area, encompassing both the Crane (solid outline) and Harney Basin (dashed outline). Note the presence of north-south trending topographic escarpments in the study area (white box, Figure 4). Shown are the westward younging isochrons of the High Lava Plains silicic volcanism (Jordan, 2004) and the estimated locations of the eruptive centers for the largest HLP eruptions [DC: Devine Canyon 9.63 Ma; PC: Prater Creek 8.41 Ma; RS: Rattlesnake 7.04 Ma] (Jordan 2004, Streck 1999).

opment of this region at the margin of Basin and Range which is key to defining how a continental extensional province develops, evolves and migrates.

Goals of this study are to address the following questions:

- When did the Northwestern Margin of the Basin and Range form?
- How did the margin develop in both space and time?

- What historical relationship exists between the structural development of the Basin and Range and the magmatic history of the High Lava Plains?

## Methods

Field mapping of the study area was undertaken at 1:24,000 scale using a topographic base. Cataloging of sample locations and points of observation was aided through use of a Garmin eTrex GPS unit. The stratigraphic record of the Crane Basin includes alternating volcanic and sedimentary units, which constrained the age of fault activity and basin development. Measured stratigraphic sections were taken using a 5-foot Jacob staff and a Leitz inclinometer to provide thickness, facies and contact relationships for the basin fill (see Appendix for complete measured sections).

Whole rock samples were analyzed for chemical compositions at Washington State University's analytical lab. Major elements were analyzed using XRF while minor and trace elements were analyzed on the ICP-MS. Age dates ( $^{40}\text{Ar}/^{39}\text{Ar}$ ) were done at Oregon State University Noble Gas Mass Spectrometry lab in the College of Oceanic and Atmosphere Sciences. This combined information was used to construct cross-sections along five profiles to provide a three-dimensional geometry of the Crane Basin, and quantitative estimates of fault displacement and rates.

## Regional Stratigraphy

The study area includes the following Cenozoic mapable units; the Steens Basalt, rhyodacite intrusions and domes, three tuffaceous sedimentary units, the Dinner Creek, widespread Devine Canyon, and Rattlesnake ash-flow tuffs, the three localized basalt flows and an isolated scoria cone deposit (Figure 4). The Miocene age Steens Basalt is the basal Cenozoic rock unit.

The greater Crane Basin, defined by the preserved volcanoclastic sediments, was divided into two small sub-basins within the study area. This was done to separate the 9.63 Ma to 7.25 Ma sedimentary deposits, which geologic mapping suggest were deposited in different and isolated depocenters, but interpreted as chronostratigraphic correlatives. In the east are the Eastern Crane Basin sediments (Tst unit) and in the west are the Western Crane Basin sediments (Tsts unit).

### **Steens Basalt: Tba**

**Location and Contacts:** The most widespread and oldest unit in the Crane Basin study area is the Steens Basalt, which has an age ~16.5 Ma (Swisher, 1990). The total thickness of this unit is indeterminable in the field area because the base is not exposed. The thickest exposed sections are >300 meters thick on the western side of the Little Crane Creek drainage.

**Unit Description:** The Steens Basalt often forms rounded, irregular outcrops of lava flows, low-relief hills that appear reddish to rusty brown in color, and include poorly developed paleosol layers between flows. Individual flows, when exposed vary in thickness from 5 to 15 meters thick. Flows are assumed to have been deposited with relatively low slopes. The basalt is phaneritic, to occasionally aphanitic with subhedral to anhedral ortho and clino-pyroxenes groundmass, a minor fraction of anhedral plagioclase phenocryst, and is moderately to very vesicular in hand sample.

### **Dacitic intrusions and rhyolitic flows: Trd**

**Location and Contacts:** Rhyodacites are found along Crane Creek, Swamp Creek, and west of the Coleman Creek fault where they are exposed as rounded, topographic highs ranging in age from ~15 Ma to 9.5 Ma (Fiebelkorn, 1983; Walker, 1979). Intrusive contacts between rhyodacite intrusions that feed domes and Steens Basalt are marked by a flow-foliated,

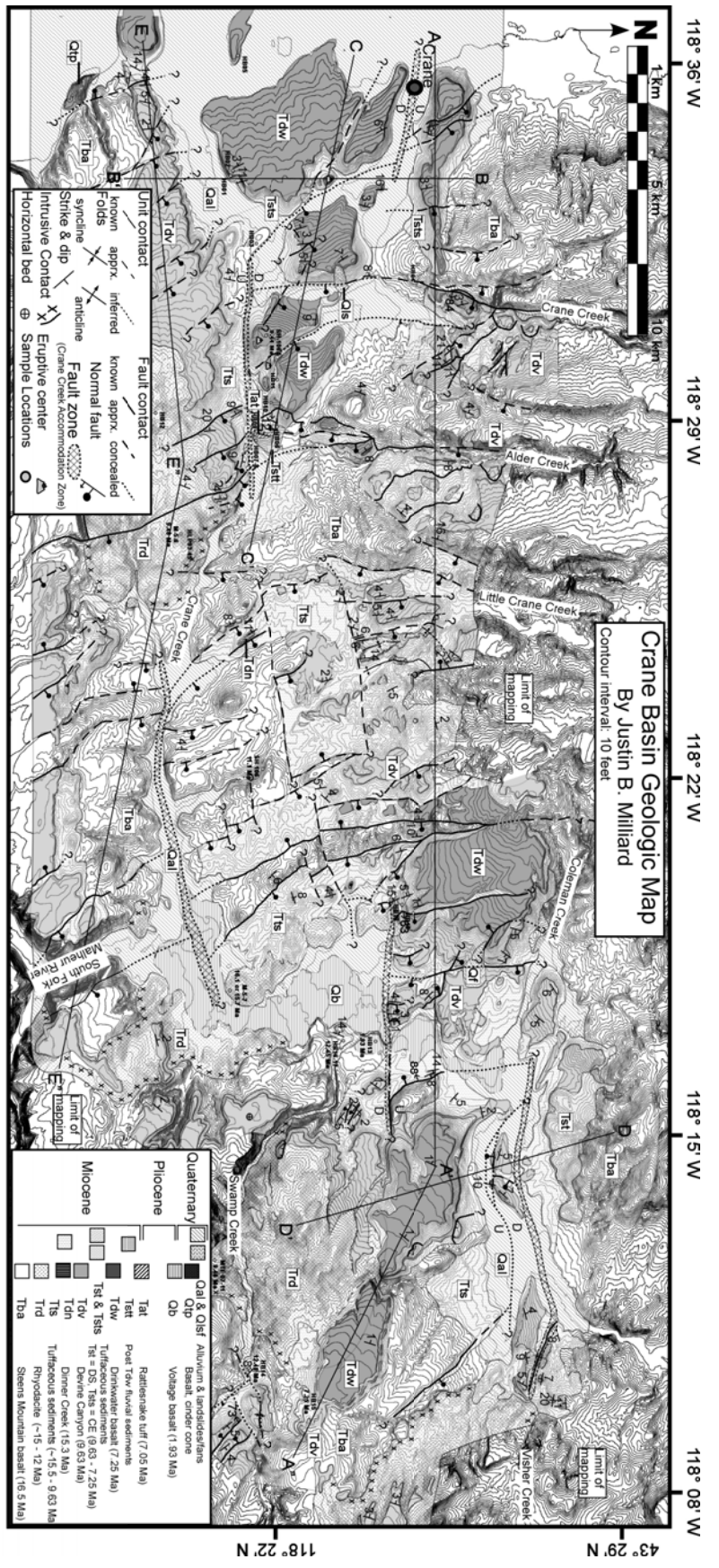


Figure 4. Geologic map of the Crane Basin study area. Unit notations were adapted from Walker (1972). Lines of cross section in Figure 8 are shown. Samples and their respective ages are shown, non Harney and Crane Basin samples are mapped as reported by Fiebelkorn (1983)



quenched margin. Rhyodacite lava flows on the eastern margin of the study area are on the order of tens of meters thick.

**Unit Description:** Colluvial float of rhyodacite is pervasive in the sedimentary record and is limited to flow banded cobbles with aphanitic and equigranular grains whose source location are indeterminable. At Visher Creek a vitrophyre forms distinct black cliffs, often with distinguishable columnar jointing. Samples are aphanitic and often porphyritic with subhedral quartz phenocrysts.

Field relationships where intrusive contacts are subvertical suggest that rhyodacitic intrusions often breached the Steens Basalt plateau surface as domes to form topographic highs, an interpretation currently supported by the fact that they remain today as the dominant topographic highs. The lithology of fluvial cobbles found within the axial drainages of the Crane Basin are dominantly >95% rhyodacitic, supporting the interpretation of the domes being the paleo-topographic highs and the source of fluvial drainage systems.

### **Crane Basin volcanoclastic sediments: Tts**

**Location and Contacts:** Defining the dimensions of the Crane Basin are the widespread, mid-Miocene volcanoclastic Tts sediments. Crane Basin sediments disconformably overlie the pre-faulted rocks of Steens Basalt and rhyodacite intrusions and domes. Contacts are often hard to discern due to the unit's unconsolidated nature. It forms broad transitional contacts where the sediment thins and forms veneers over underlying bedrock. Overlying the Crane Basin sediments is the 9.63 Ma Devine Canyon tuff whose exposure aids in defining the extent of Tts sediments. The depocenter itself is irregular in shape, being the composite of numerous interconnected half-graben basins filled with sediment. Therefore the basin does not have a uniform thickness. Each basin has a sediment column that thickens towards the fault trace and

thins toward the hanging wall where it onlaps underlying bedrock. As each younger layer is deposited, the basin margin progrades away from the fault as new layers “onlap” the pre-faulted rocks of Steens Basalt or rhyodacite.

**Unit Description:** Crane Basin sediments crop out poorly and typically appear as recessive slopes below the overlying competent Devine Canyon tuff. Crane Basin sediments are poorly lithified to moderately lithified and appear white to light gray to a light tan color. These colors are readily apparent in outcrop when contrasted to the red/browns of the Steens Basalt bedrock. Differentiation between Crane Basin sediments, and the younger Western Crane Basin sediments (Tts) and Eastern Crane Basin sediments (Tst) is difficult because their outcrop color and textural characteristics are similar. Differentiation is based upon stratigraphic position.

Lithologies for Crane Basin sediments range from extremely fine grained monolithic claystones to siltstones, to air-fall tuffs, polyolithic sandstones and pebble conglomerates, to cobble breccias and conglomerates. Petrology of lithics is dominated by silicic material, likely derived from nearby rhyodacitic outcrops. Cobbles in fluvial deposits are exclusively comprised of rhyolite and are adjacent and parallel to fault traces, suggesting that drainage networks were fault controlled. Pebbly, basaltic sandstone beds are also present but less common. Fossils were found at two separate localities within Tts during this study; lacustrine gastropods and an astragalus from an artiodactyl, a species of camelid (Fremd, 2008). The mid-Miocene age of the camelid fossil is contained within the bracketed age of the unit. Interbedded with the secondary volcanic sediments were primary volcanic deposits of air-fall ash and rhyolite lava, which were utilized to calculate a sedimentation rate within the Crane Basin and extrapolate the timing of initial deposition of the Tts unit.

By calculating the sedimentation rate for the basin between the time of the interbedded volcanic marker beds and the overlying Devine Canyon tuff an estimation for the time of initial deposition in the Crane Basin could be calculated. This was done by measuring the thickness of sediments from the marker beds to the basal contact of the unit and then dividing this by the rate of sedimentation. The first of the two marker beds discovered within the Crane Basin sediments is a direct air-fall tuff is composed of >90% glass shards, with minor plagioclase. This ash has yet to be described in the literature and is located in the eastern portion of the Crane Basin. The lower 1.5 meters of the ash is a massive bed with normal grading, asymmetric ripples and the infrequent planar bed. The upper 1.5 meters is upward thinning, planar beds of ash. Two samples of the ash were collected from separate localities for dating. The newly discovered air-fall tuffs are interbedded within the previously described Tts unit of Walker (1979) is here termed Swamp Creek Ash. Both samples overlie a basaltic pebbly sandstone couplet, the only mafic bed observed in the Crane Basin strata which suggest that both samples are regional correlatives. An  $^{40}\text{Ar}/^{39}\text{Ar}$  age determination for Sample HB14's weighted plateau age is  $12.48 \pm 0.13$  Ma and sample HB17's is  $12.45 \pm 0.13$  Ma (Figure 5).

The depositional environments of the Crane Basin sediments vary widely, from landslides and mudflows to river and stream systems to lakes and playas. The landslides and mudflows characterize mass wasting events at the fault bounded margins of the basin and are represented by the conglomerates and breccias recorded in stratigraphic section 2 (appendix). The river and stream systems are represented by silicic detritus rich sandstones, pebbly conglomerates and cobble conglomerates. Suggesting that sediment was sourced from Trd domes and lava flows then transported to the regional depocenter. The lakes and playas are represented in the rock record by claystones, mudstones and evaporates.

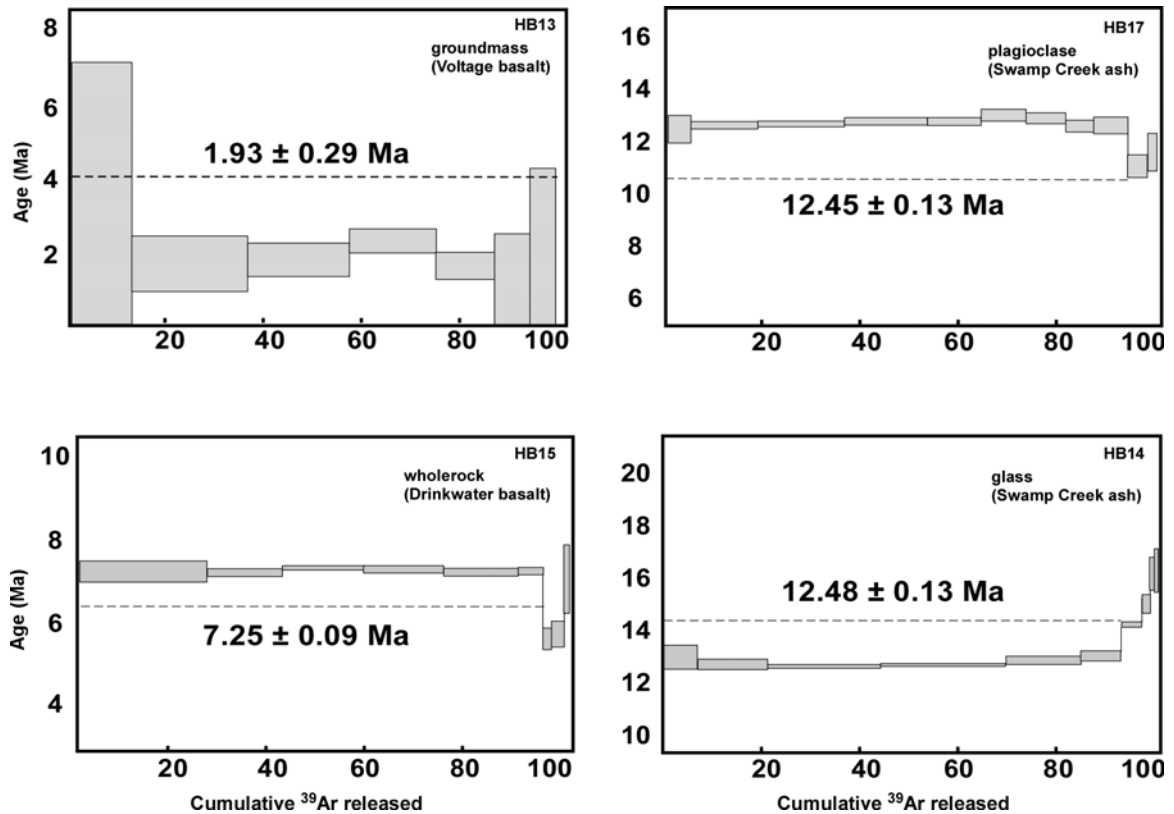


Figure 5.  $^{40}\text{Ar}/^{39}\text{Ar}$  age plateaus for dated samples.

### Devine Canyon ash-flow tuff: Tdv

**Location and Contacts:** The 9.63 Ma (Ford, 2009) Devine Canyon ash-flow tuff is the key unit to understanding the Crane Basin because it was instantaneously deposited within the Crane Basin and it forms a resistant caprock. Thus, the basin geometry and topography at the time of eruption is well preserved. Tdv overlies Crane Basin sediments in the depocenters and on the basins margins Tdv overlies Steens Basalt or Trd rhyodacite. This relationship indicates Crane Basin sediments onlap in distal locations relative to basin bounding faults. The Devine Canyon tuff thickness varies laterally from 5 to 15 meters.

**Unit Description:** The Devine Canyon tuff is resistant, forming cliffs and rim rock that vary in color between gray to buff and weathers a pinkish red. The defining characteristic of the unit in the study area are the large, oblate, 4 to 14 cm diameter, black fiamme. The layer immediately below the welded section is white to yellow, pumaceous gravel, 3-5 cm in diame-

ter. The ignimbrite is devitrified, highly welded, gray to green-gray to black glassy groundmass, very coarse grained with various lithics, including easily recognizable black obsidian.

### **Crane Basin syntectonic sediments: Tst (east) & Tsts (west)**

**Location:** These units are chronostratigraphic corollaries representing Crane Basin deposition from 9.63 to ~7.25 Ma, but are differentiated because they were deposited in isolated sub-basins. Field evidence suggests that the Eastern Crane Basin was separated from the Western Crane Basin by a structurally controlled topographic divide formed before or at the time of the Devine Canyon eruption by the uplifted footwall block of the Coleman Creek fault.

#### **Tst: sediments of the Eastern Crane Basin**

**Unit Description and Contacts:** The basal contact of Tst rests atop the Devine Canyon tuff although it onlaps the country rocks of Steens Basalt (Tba) and rhyodacite (Trd) locally. Conformably overlying Tst is the Drinkwater basalt (Figure 6A). The thickest section of Tst is roughly 110 meters.

Due to poor exposure, no appropriate sections were discovered to be described and measured. In scattered outcrops the unit appears white to tan to orange in color, forms slopes, and is deeply incised in drainages. The limited outcrops observed suggest that the unit is dominated by volcanoclastic sandstones, siltstones and mudstones. The associated detritus is largely silicic in composition, and subangular to subrounded in shape.

#### **Tsts: sediments of the Western Crane Basin**

**Unit Description and Contacts:** The basal contact of Tsts is unconformable resting atop the Tts and Tba, an erosional surface. In some locations the basal contact is conformable, where Tsts is clearly deposited on Tdv, forming a normal succession of strata (Figure 6B). Drink-

water basalt conformably overlies Tsts. Stratigraphic section 1 (appendix) represents a near full measured section of Tts at its eastern limit, where it is approximately 153 meters thick.

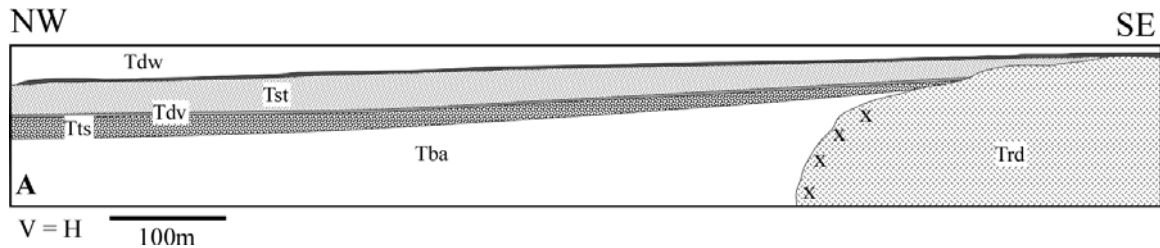


Figure 6A. Partial cross section taken from the A'-A'' transect that illustrates the structural relationship of the Crane Basin units [Tba: 16.5 Ma Steens Basalt; Tdv: ~15.5 Ma – 12 Ma rhyodacitic domes and flows; Tts: ~15 Ma – 9.63 Ma Crane Basin sediments; Tdv: 9.63 Ma Ma Devin Canyon tuff; Tst: 9.63 – 7.25 Ma Eastern Crane Basin sediments; Tts: 9.63 – 7.25 Ma Western Crane Basin sediments; Tdw: 7.25 Ma Drinkwater basalt. The conformable relationship of the units in the Eastern Crane Basin is displayed where they onlap onto the country rocks at the basin's margin. The structural relationship represents a continuous record of sedimentation as the basin progressively fills.

The unit crops out as recessive slopes, and is poorly exposed. Color varies from white to buff, to yellow to brown. Exposures are best within incised drainages and along railroad grades. The lithology is dominated by monolithic breccias, conglomerates, and sandstones that are primarily silicic in lithology. Pumice gravels abound, the largest of which has westward prograding foresets >1m tall. Paleo-flow indicators within this section collectively suggest a flow direction ranging from southwest to northwest. Numerous intrusions of basalt cross-cut Tts, which often occur as sill-form bodies that intrude along bedding. Intruded basalts possess spherical spalling. The dikes represent part of the feeder system for the overlying Drinkwater basalt.

The depositional environment of Tts was likely a fluvial / deltaic system that fed the Harney Basin depocenter. The aerial exposures of the unit suggest that it was deposited in an embayment on the eastern limit of the Harney Basin. Chronostratigraphic corollary deposits of

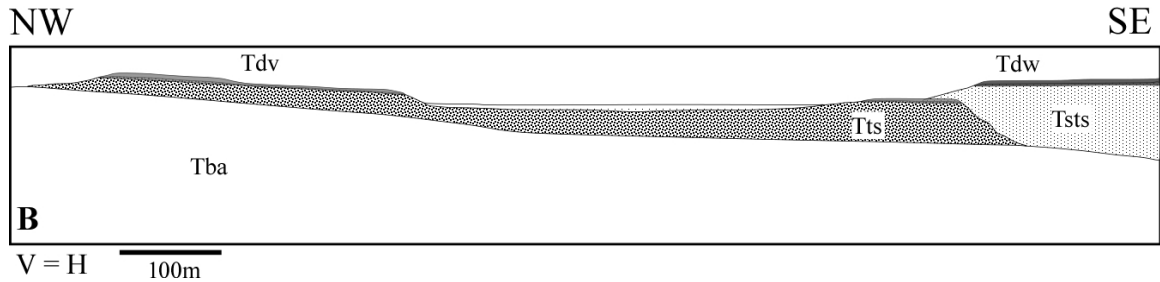


Figure 6B. Partial cross section southern portion of the B-B' transect. Here the unconformable relationship between Tsts and older units is most easily recognized. This contact represents an erosional surface where the Tdv and Tts were incised into and evacuated westwards. Later that surface was later deposited upon by younger Tsts sediments as the Harney Basin filled. Analogous relationships are found elsewhere in the Western Crane Basin, recording the rapid subsidence and infilling of the Harney Basin during the late Miocene.

Crane Basin Tst and Tsts volcanoclastic sediments are found to the northwest, where they exist stratigraphically above the Devine Canyon tuff and below the Rattlesnake tuff as presently mapped (the Prater Creek tuff is mapped to be interbedded within these sediments) (Greene, 1972). Suggesting that the depositional sequence within the Crane Basin continued across the Harney Basin.

### Drinkwater basalt: Tdw

**Location and Contacts:** Two flows of Drinkwater basalt occur in the Crane Basin study area, one in the Eastern Crane Basin and one in the Western Crane Basin. The Drinkwater basalt conformably rest atop Tst and Tsts sediments of the Crane Basin. At the margins of the depocenter the Drinkwater basalt onlaps Tba bedrock.

**Unit Description:** The thickness of both flows varies laterally but is generally 5 to 8 meters thick. The Drinkwater basalt forms distinct black to brown cliffs and rimrock in the field area. Flows are vesicular at their base, with vesicles rapidly decreasing upwards through flows. The basalt is aphanitic, equigranular, diktytaxitic in texture, with minor phenocrysts of anhedral

olivine and pyroxenes. Within stratigraphic section 1 (appendix) basalt dikes and hyrdoclastite are found that intrude upward through the sediments. At the top of the section, the Tsts/Tdw contact is marked by mafic agglomerate, where pyroclastic basalt bombs, blocks, and debris are conformably deposited atop Tsts pumice sediments. In the Western Crane Basin, a correlation between the location of Drinkwater eruptive centers and faults can be inferred. The identifiable eruptive centers for Tdw basalt occur along the mapped fault traces of half-graben forming normal faults, suggesting that the developing fault systems provided weakened conduits to be exploited by High Lava Plains magmatism.

### **Volcaniclastic sediments: Tstt**

**Location and Contacts:** Field evidence suggests that following the eruption of the Drinkwater basalt within the Western Crane Basin a period of rapid incision ensued. This is structurally represented by unconformable contact between the <7.25 Ma Tstt and the 7.25 – 9.63 Ma Tsts in the Western Crane Basin. A complete stratigraphic sequence would have Tdw conformably overlying Tsts and then Tstt conformably overlying Tdw. Thus, this unconformity suggests a small valley formed in the Western Crane Basin following 7.25 Ma. This incised valley was filled with cobble and pebble gravels of Tstt that are described in detail in stratigraphic section 7. Gravels lie atop both Tsts and Tba (inferred contact at depth) and are overlain by the 7.04 Ma Rattlesnake tuff. The measured thickness of the unit is roughly 27 meters.

**Unit Description:** The unit forms slopes that are littered with well-rounded cobble float. In outcrop there are clast-supported gravels, with little to no cement. Gravels vary between felsic rich, with banded rhyolites, obsidian, and pumice to mafic rich, with >90% basalt clast. The presences of basalt clast dominated beds is unique to stratigraphic section 7 and have yet to be found elsewhere in the field area. Clasts range in size from sand to pebbles to



large cobbles (>20cm in diameter). The clasts are well to very well rounded. Hand sample analysis of basalt clasts suggest they are derived from the Drinkwater basalt. This serves as to further support interpretation of having a valley incised through the Drinkwater basalt between 7.25 and 7.05 Ma to be later filled in with fluvial gravels and the Rattlesnake tuff.

The depositional environment can be inferred to be fluvial, from the abundance of well-rounded, imbricated clasts, unlithified matrix, and clast-supported gravels. Westward dominant imbrications also support an east to west flowing stream that incised across the earlier-deposited Tsts sediments.

### **Rattlesnake tuff: Tat**

**Location and Contacts:** Exposures of the 7.05 Ma Rattlesnake tuff are present in the Western Crane Basin. These exposures were initially identified in the field based upon the black and white pumice within them; a defining characteristic of the Rattlesnake tuff (Streck, 1995). There are two identified outcrops of Rattlesnake tuff in the field area, the northern outcrop overlies the Tstt unit and both dip westward at a similar angle.

**Unit Description:** The Rattlesnake tuff is approximately 8 meters thick. The Rattlesnake tuff forms a visible outcrop but not a definitive cliff band. It weathers a yellow-brown-orange on well-exposed surfaces but is gray to white on fresh surfaces. There is a lower, poorly welded section that is graded from light gray at the base, upward to dark gray in color, with >70% ashy matrix with various lithics of glass and pumice. The pumice is largely white in color, but occasionally gray and banded white/black pumice exists.

**Geochemical Analysis:** Geochemical data demonstrate that this is the Rattlesnake tuff by correlating the trace element geochemistry of High Field Strength elements between sample HB09 and the known geochemistry of Rattlesnake tuff (Figure 7). Representative samples of

Devine Canyon, Prater Creek and Rattlesnake tuffs were chosen for comparison that had known  $^{40}\text{Ar}/^{39}\text{Ar}$  dates conclusively identifying them. Streck found 5 distinct variations of Rattlesnake tuff pumices (Groups A – E) (Streck, 1995, 1999a). End members A and E were used in this study. The intention of the experiment was to constrain if HB01 or HB09 was a possible Rattlesnake tuff sample by seeing if its geochemistry fell between Streck's A and E endmembers. Comparison of chemistries focused strictly upon the less mobile, High Field Strength elements (Y, Hf, Zr, Ti, Nb, Ta) (Rollinson, 1993). Analysis was limited to these elements due to the evidence of alteration to sample HB09 seen in the low totals of the un-normalized major elements (HB09 87.04 weight %, see appendix). HB09 is anomalously high in the compatible elements (likely a result of alteration via weathering), but it has anomalously low values in many of the incompatible elements. Though, when HB09 geochemistry does match up with values of other samples it is most often RT165E or RT134A, such as Nb, Ta, and U. HB09 and RT344 are the only samples with high Ba. By combining both the field and geochemical evidence, we can confidently assert that sample HB09 is the Rattlesnake tuff.

The depositional environment of a paleo-channel or canyon is preserved by the anomalous nature of the Rattlesnake deposit here in the Western Crane Basin. The Rattlesnake eruptive center of the ash-flow is ~100 km to the west of the Crane Basin and no other exposures of it exist this far eastward. Field relationships suggest that the Harney Basin was topographically much lower at the time of the eruption, and it is interpreted that the eastward flowing ash-cloud would have slowed in this depression. It would not have the kinetic energy to overcome the topographic high to the east except where the high was incised to, allowing only traces of the flow to continue eastward. Hence, why there is only this exposure of Rattlesnake tuff eastward of the present Harney basin.

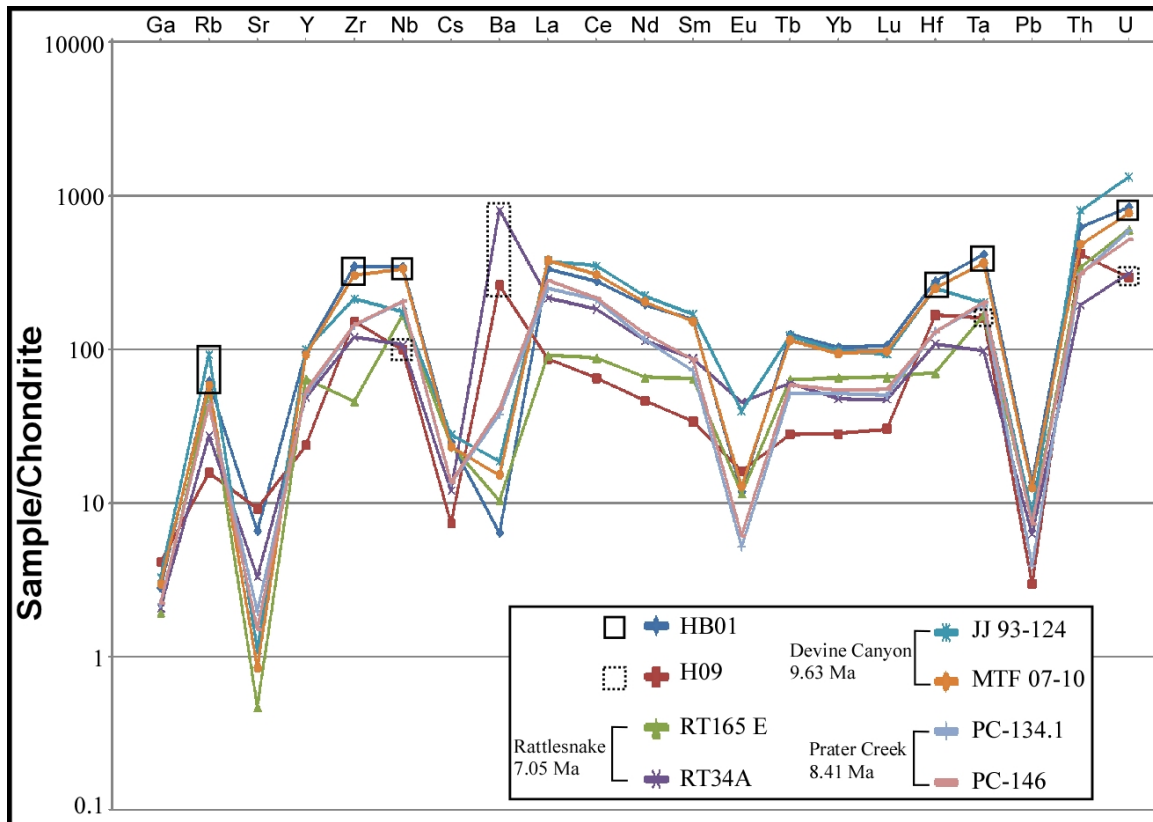


Figure 7. Spiderplot comparing the two unidentified Crane Basin ignimbrite pumice samples, HB01 and HB09, to the geochemistry of dated and identified samples of the three largest HLP ignimbrites, the Rattlesnake (RT165E & RT34A) (Streck and Grunder, 1995), Prater Creek (PC-1341 & PC-146), and Devine Canyon (JJ 93-124 & MTF 07-10)(Ford, 2009; Johnson, 2000). The closest matched High Field Strength elements are outlined. HB01 matches the Devine Canyon tuff chemistry and HB09 matches the Rattlesnake tuff chemistry.

### Voltage basalt: Qb

**Location and Contacts:** The youngest unit in the Crane Basin is the  $1.93 \pm 0.29$  Ma

Voltage basalt (Camp, 2003) which is found along the south fork of the Malheur River valley, outcropping from the southern margin of the Harney Basin to the northern margin of the Eastern Crane Basin. The basal contact conformably overlies older Quaternary fluvial sediments and unconformably overlies Tba and Trd bedrock. Younger unconsolidated sediments, both onlap and cover the basalt flow. Thickness of the flow is approximately 5-7 meters. The Voltage Flow within the Crane Basin has been mapped by previous authors as part of the larger Voltage flow that originated south of the town of Voltage, Oregon in the southeastern corner of

the Harney Basin (Greene, 1972; Walker, 1991). The farthest toe of the related flow extends downstream, northward past the Crane Basin field area roughly 85 km away. Previous dates were calculated from samples collected around the main flow that range from 1.23 Ma to 1.6 Ma (Jordan, 2001). The Voltage basalt occupies the bottom of the south fork of the Malheur River canyon. Which flows northeast away from the Harney Basin, suggesting a paleo-south fork of the Malheur River exists prior to the eruption.

**Unit Description:** The Voltage basalt forms a basalt plain with preserved tumuli and pressure ridges. The flow is aphyric and porphyritic, dikytaxitic textured basalt. Geochemistry was done on this unit as well but not used in interpretation during this study. Samples collected near the eruptive center by previous authors suggest the samples are related (Carlson, 2009).

## **Qal**

The Quaternary alluvium (Qal) of the study area exists in two separate drainage basins; the present Harney Basin to the west, and the south fork of the Malheur River to the east. Separating these two drainage basins is a bedrock drainage divide, located due east of the town of Crane. It is a mere 18 meters above the average water level of Malheur Lake. It is important to note this because prior to ~1.9 Ma ago during the period of the Voltage basalt eruption, the Harney Basin drained externally until its exit was dammed by the Voltage basalt flow. As a result, the erosional surface within the Harney Basin has since been back-filled with subsequent alluvium during numerous Holocene glacial periods. Extrapolation from field evidence suggests that Qal filled in topography created by incised Tsts within the Harney Basin. Based on the present exposure of the Voltage flow eruptive center, Qal depth does not likely exceed 10 meters.

To the east, in the majority of the Crane Basin study area, Qal forms a thin veneer upon older bedrock within stream channels.

## **Cross-Sections**

### **Methods**

Five cross-sections were constructed in the Crane Basin to illustrate the structural geometries across the field area and to calculate the amount of east - west extension across the fault fabric (Figure 8). Field evidence and map relations indicate that the fault geometry reflects a series of north-south fault bounded half-graben depocenters. The method of measuring fault offset depends on the interpreted mode of faulting. Schlische (1991) proposed three end-member models for fault geometry and half-graben development that were considered for use in this analysis. These three models are: detachment fault, domino-style, and fault growth. All three were reviewed, but only the domino-style model was employed (Figure 9). The domino-style model best reflects the fault geometries and field relationships recorded in the Crane Basin. The majority of faults dip the same direction, are rotated similar angles and are connected by an east-west striking transform fault. These are characteristics that define the domino-style model. This model was well documented by Proffett (1977) in central Nevada, where it was the ideal fit for Basin and Range style extension. Also essential to this model is the assumption of uniform strain, which requires that basins to be bounded by along-strike transfer faults (ie. The Crane Creek Accommodation Zone) and that the rate of increase in the basin volume is negative. As the depocenter matures the rate at which sediment fills it in decreases with time and when employing the domino-style model one expects as the basin matures the system to evolve from a closed lacustrine depocenter to a through-flowing fluvial system.



As the basin develops the rate of volume growth controlled by subsidence decreases relative to the rate of sediment input and aggradation. This negative relationship results in a basin in which the supply of sediments exceeds the capacity of the basin, causing a shift from lacustrine to fluvial sedimentation (Schlische, 1991). This serves to support the Crane basin is an immaturely developed Basin and Range mode of extension. This relationship could not be established through stratigraphic sections alone, due to the poor exposure, but the basin evolution of both the Harney Basin and Crane Basin exhibit the lacustrine to fluvial evolution. This evolution is discussed later, but can be summarized by an aggrading, lacustrine depocenter that evolves into a self-evacuating fluvial system.

Two cross-sections, cross-section A-A'-A'' and C-C', were chosen for quantitative analysis of fault displacement and extension rates. These cross-sections cut two faults, the Crane Creek and Coleman Creek faults that preserve four key stratigraphic relationships that constrain the reconstruction of fault activity in time.

Fault dips were generalized to a similar 70° dip for ease of analysis, though fault dips were attained on numerous Pliocene age-fault escarpments in Crane Basin field area ranging from 70° to 90°. Similar fault dips have been documented in other Northwestern Basin and Range studies (Pezzopane, 1993; Scarberry, 2008; Trench, 2008). The domino-style model assumes that all faults slip and rotate concurrently. The only exceptions to 70° east dipping faults were the antithetic faults or small-offset synthetic faults within the larger domino fault blocks (ie. fault 13).

Cross-sections were drafted at a 1:24,000 scale. Cross section A-A'-A'' traverses the northern margin of the Crane Basin field area, transecting four large offset faults forming their respective present-day drainages. Listed from west to east these are: Crane Creek, Alder Creek,

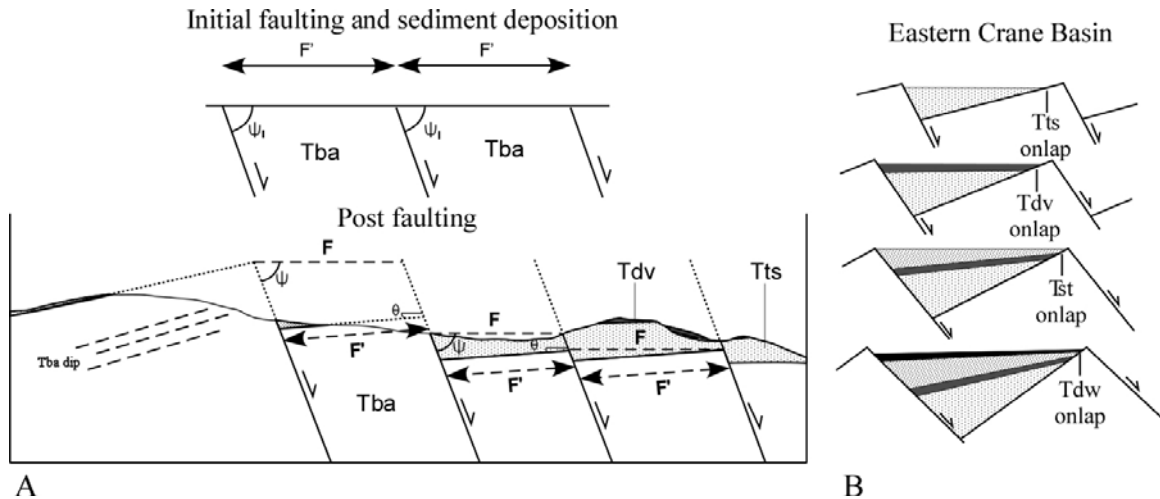


Figure 9. A) **Schematic** domino-style fault geometry model of Schlische (1991) and Wernicke (1992) adapted and utilized for this study. The upper diagram is a schematic cross-section of the earliest stage of Crane Basin development, where  $\psi_i$  is the initial dip angle of the faults and  $F'$  is the initial fault spacing immediately following the initial Tts deposition. The lower diagram is a partial cross section from A – A' in the Little Crane Creek drainage (Figure 4 & 8), where  $\psi$  is the fault dip after extension,  $\theta$  is the dip of the 'assumed' originally horizontal contact between Tba and Tts, and  $F$  is the fault spacing after extension. B) Filling model for domino-style half-grabens modified from Schlische (1991). Time progression from top to bottom, with each successive unit, Tts – Tdv – Tst – Tdw, onlapping the hangingwall block. Model shows the idealized depositional relationships found in the Eastern Crane Basin in Figure 10.

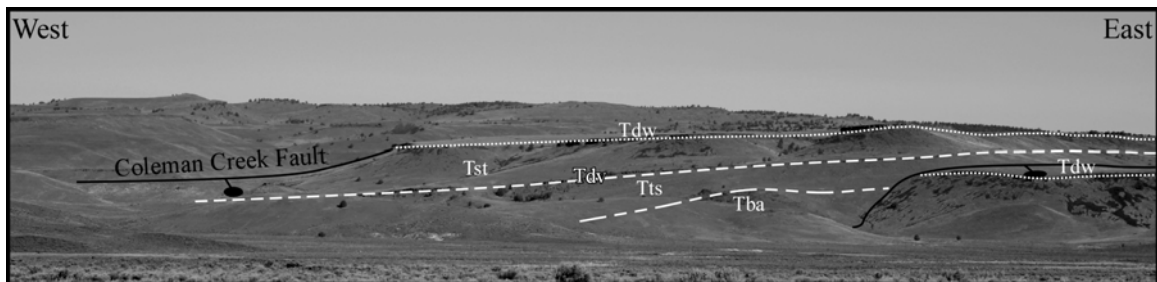


Figure 10. View looking northwest at an outcrop within Eastern Crane Basin where a complete stratigraphic section is visible, showing the exposed eastward thinning strata as displayed in Figure 9B.



Little Crane Creek and Coleman Creek. All four drainages, except Alder Creek, lack a solitary fault trace, but contain numerous accompanying synthetic and antithetic faults. Although smaller faults were mapped, the vertical component of separation is largely accommodated for by the sole basin-bounding fault. Domino-style fault analysis was employed on faults that preserved Tts sediment and could be assumed to be active as early as the mid-Miocene (~15.5 Ma), including faults 5 (Coleman Creek), 8, 9, 10, 11 (8-11 compose the greater Little Crane Creek fault system), 12 (Alder Creek), 14, and 15 (Crane Creek). Faults 6, 13 and two west-dipping faults east of fault 6 were ignored in the domino-style faulting analysis as they are small-offset synthetic and antithetic faults contained within their greater domino blocks.

Horizontal extension was calculated by employing the method of Wernicke (1982).

$$\beta = \left( \frac{F}{F'} \right)$$

**Equation 1.**

Dividing the present horizontal distance between faults (F) by the original horizontal distance between faults (F'), horizontal extension can be derived ( $\beta$ ) (Equation 1). The original horizontal surface that represents pre-fault geometry is assumed to be the initial depositional contact between Tts and Tba. It is noted that this initial parameter assumes that the region possessed a similar base level at the initial time of deposition within the greater Crane Basin, but it is still the best constraint for the timing of initial fault activity (~15.5 Ma determined by sedimentation rate analysis discussed in Tts section).

## Local Structural Framework

A first-order observations of the field area reveals that the region north of the Crane Creek stream channel possesses defined topography, with dominant north to south trending topographic escarpments. To the south of the stream channel, topography is subtler, with fewer topographic escarpments, which possess relatively less displacement compared to their correlatives to the north. This relationship suggests that the northern region has undergone more extensional faulting when compared to the southern region. The zone separating these two regions is marked by the east to west trending Crane Creek stream channel which joins the south fork of the Malheur River. The Malheur River forms a broad north to south trending river valley until it reaches the center of the eastern Crane Basin at which point it turns 90° eastward, and forms a distinct east - west trending valley. A closer look at the tributaries of the previously described main stream system reveals the largest tributaries all drain from the northern region in north - south trending valleys. This is a textbook example of a trellis drainage pattern highlighting the greater topography to the north, which suggests greater displacement upon northern structures.

These first-hand observations of differential extension to the north and south of the Crane Creek stream channel require a mode for accommodation. Though direct exposure is lacking, numerous relationships suggest the presence of an east to west trending accommodation zone between the northern, highly extended region, and the southern, less extended region. The Crane Creek Accommodation Zone is a series of east - west trending transform fault zones that connect to each other through a series of north - south normal faults, forming distinct T-junctions, which results in the trellis drainage pattern. A less explored observation, but equally important, is the limitation of rhyodacite (Trd) to the southern and eastern region of the field area. The rhyodacite exist on only the southern side of the Crane Creek Accommoda-

tion Zone. Lavallée (2009) found that volcanic edifices in southern Peru preferentially positioned themselves at intersections of north - south trending normal faults, and northeast to southeast strike-slip faults. Lavallée (2009) suggested that this is possible that this is because brittle deformation caused "crustal gaps" to form at the corners of these intersections. Similar findings have been observed at Crater Lake and Newberry Crater, both in Oregon where volcanism is thought to have been focused at the tips of the grabens due to block rotation and crustal openings caused by strike-slip motion (Goldfinger, 1997 ; Gutmanis, 1989; Lavallée, 2009). At a minimum, the mapping done in the Crane Basin study area provides evidence that extensional strain was accommodated by two deformational mechanisms, brittle and intrusive. To the north of the Crane Creek Accommodation Zone, normal faulting accommodates ~6% extension, while to the south of the Crane Creek Accommodation Zone, faults account for only ~1% of extension. Hence, rhyodacite intrusions which are similar in age to the extensional structures may have accommodated for the remaining ~5% of extension. This observation suggests that a direct and important link exists between the region's extensional deformation and its inter-crustal/subcrustal magmatism.

### **Scissor-type Normal Faults**

A characteristic defining the normal faults in the Crane Basin is their scissor-type geometry. Maximum displacement occurs at the junction of a north - south normal fault and an east - west tear fault in the Crane Creek Accommodation Zone, and displacement decreases northwards moving away from the tear fault. This relationship is clearly exhibited at the Coleman Creek fault where the youngest stratigraphic unit, Tdw, goes from more than 80 meters of vertical displacement in the south to zero in the north.

A comparison between the analysis on the A-A'-A'' cross-section and the analysis on the C-C' cross-section is possible because the same faults are transected by both sections. Field relations support that faults 1, 2, and 3 of C-C' correlate to faults 14, 15 and 18 of A-A'. The combined amount of extension across the C-C' faults is 285 meters, which represents 3.7% extension, while across the A-A' faults where roughly 147 meters of horizontal extension has occurred representing ~1% extension. It is important to note that the A-A' analysis incorporates all deformation from ~15.5 Ma onward while the C-C' analysis only includes the post 7.25 Ma Drinkwater deformation. This analysis clearly illustrates the previously mentioned scissor-type fault model for the Crane Basin, where displacement on the normal faults increases towards a the Crane Creek Accommodation Zone.

## Results

### **Total Extension**

Total horizontal displacement along the A - A' - A'' cross-section calculated through the domino-style analysis is estimated to be 1,410 meters. The total horizontal length is ~21,787 meters, the restored length is 20,377 meters, and so an estimated 6.9% extension has occurred from the Crane Creek Fault (fault 15) to the Coleman Creek Fault (fault 5) since ~15.5 Ma. This analysis takes into account only the aforementioned large-displacement, domino-style faults that fit the model and are interpreted to be connected at depth. Smaller faults are assumed to be limited to within each domino fault block.

By combining the analysis on the domino-style faults with the additional synthetic and antithetic faults (16, 17, and 18 to the west and 1, 2, 3, and 4 to the east), a total of 1,520 meters extension has taken place from A to A'. The total horizontal length is ~33,675 meters, and the restored length is ~32,155 meters. This provides an estimate of 4.7% extension has taken

place since deposition was recorded to have begun at ~15.5 Ma, a rate of approximately 98 m/Myr, and a strain rate of .003 m/Myr.

## **Fault History**

### **Stratigraphic Constraints on the Onset of Extension**

By utilizing both the Visher Creek rhyolite lava and the Swamp Creek Ash as dated horizons within the Tts stratigraphic column a deposition rate could be calculated to estimate the timing of initial deposition of the sediments upon the bedrock. In theory this would represent the fault initiation, subsidence of the depocenter, and basin formation. Thickness of sediment was measured between the overlying Devine Canyon tuff, the dated beds and the basal contact at the two sites.

Site one, located along the upper Swamp Creek, is a smaller isolated half-graben basin that field relationships suggest was disconnected from the main depocenter to the northwest. Roughly 36 meters of volcanoclastic sediment exists between the 12.45 Ma Swamp Creek ash and the 9.63 Ma Devine Canyon tuff, suggesting a deposition rate of approximately 13 m/Myr. This ash is roughly 3.2 meters thick and represents a moment in geologic time, therefore we do not use its thickness in the analysis. There exists roughly 41 meters of sediment below the ash that overlies the Tba. At 13m/Ma this would have taken ~3 Ma to aggrade, suggesting that deposition in the basin began at roughly 15.5 Ma.

Site two, occurs within the Eastern Crane Basin half-graben. The approximate thickness of sediments between the 9.63 Ma Tdv and the ~11.5 Ma Visher Creek rhyolite lava flow is 75 meters, yielding a deposition rate of 40.1 m/Myr. Cross-sections suggest that roughly 45 meters of Tts sediments underlie the rhyolite flow which onlap onto the Trd basement. At a de-

position rate, of  $\sim 40$  m/Myr, the basal Tts at this site is  $\sim 12.6$  Ma. This finding is supported by the fact that the Swamp Creek Ash is not found at this location.

In addition to these findings, an exposure of the 15.3 Ma Dinner Creek tuff (Nash, 2006) erupted from the Castle Rock caldera within the Lake Owyhee volcanic field (Haddock, 1967) and was identified in the Little Crane Creek drainage (Camp, 2003). The tuff at this location was deposited on the down-thrown footwall block immediately adjacent to normal fault trace and overlies older Tts sediments (Camp, 2009), hence the underlying sediments in this portion of the Crane Basin must be  $>15.3$  Ma. This information further strengthens the argument that onset of extensional related sedimentation into half-grabens occurred near basin bounding faults  $\sim 15.5$  Ma or earlier. Timing of the onset of extension in the Crane Basin is coincident with the initiation of faulting and extension in the Oregon-Idaho Graben to the east at  $\sim 15.5$ - $15.3$  Ma (Cummings, 2000), suggesting a greater regional event.

## **Timing of Extension**

### **Onset**

Fault activity in the greater Crane Basin is recorded, by the magnitude of vertical separation as the half-graben fills. Relationships in the hanging wall of the Coleman Creek fault, forming the Eastern Crane Basin and across the Crane Creek fault, forming the Western Crane Basin reveal the temporal evolution of faulting. Fault activity continued from  $\sim 15.5$  Ma up to 9.63 Ma at the time of Devine Canyon eruption, then continued to the time of the 7.25 Ma Drinkwater basalt. At this time the long-lived sedimentation patterns changed and the post  $\sim 7$  Ma fault activity is not recorded by subsequent sedimentation though it is recorded by displaced Tdw.

### **Eastern Crane Basin**

The Coleman Creek fault is a composite of a major eastward dipping normal fault which is cross-cut by a synthetic fault. The Tba and Tts contact has a vertical displacement of ~185 meters and a horizontal displacement of ~66 meters. The Tts - Tdv contact has a vertical displacement of ~460 meters and a horizontal displacement of ~195 meters. The Tst - Tdw contact has a vertical displacement of ~80 meters and a horizontal displacement of ~30 meters. Consequently, this would mean that roughly 60 meters of horizontal extension occurred between ~15 and 9.63 Ma; a rate of 10.2 m/Myr. Between 9.63 Ma and 7.25 Ma roughly 165 meters of horizontal extension occurred; at rate of 69.3 m/Myr. The 1.93 Ma Voltage basalt is not faulted. This means that roughly 30 meters of horizontal extension occurred between 7.25 and 1.93 Ma, a rate of 5.64 m/Myr.

### **Western Crane Basin**

The Crane Creek fault is similar in geometry to the Coleman Creek fault, with the exception of having a limited amount of preserved Tsts. This fact is due, in part, to the location of the preserved stratigraphic column at the northern limit of the Western Crane Basin, at the upslope margin of Tsts deposition. The basal contact between Tba and Tts has a vertical displacement of ~150 meters and a horizontal extension of ~55 meters. The Tts - Tdv contact has a vertical displacement of ~178 meters and a horizontal displacement of ~65 meters. The Tsts - Tdw contact has a vertical displacement of ~134 meters and a horizontal displacement of ~48 meters. Consequently, roughly 55 meters of horizontal extension occurred between ~15 Ma and 9.63 Ma, a rate of 9.3 m/Myr. Roughly 17 meters of horizontal extension occurred between 9.63 Ma and 7.25 Ma, a rate of 7.14 m/Myr. Following the eruption of the Tdw at 7.25, no dated units are present in the Western Crane Basin and Quaternary alluvium is undeformed. Any post Tdw

faulting ceased prior to the Quaternary (Walker, 2009). Between 7.25 Ma and 2.59 Ma, roughly 48 meters of horizontal extension occurred; a rate of ~10.3 m/Myr.

## **2-Stage Deformation**

### **Crane Basin Evolution**

By comparing the fault history on the Coleman Creek fault and the Crane Creek fault, which are interpreted to represent the east and west regions of the Crane Basin respectively, we can draw some conclusions about the region's structural development. These analyses record a ~6 Myr period when extension rates were similar suggest that deformation was evenly distributed across the Crane Basin region, which was responsible for forming the regional depocenter (STAGE 1) (Fig. 11). Coinciding with the formation of the Crane Basin during this period, both in space and time, was a larger extensional fabric which formed the mid-Miocene depocenters in southeastern Oregon. The Oregon-Idaho Graben (Cummings, 2000) formed during this same time, and is located immediately due east of the Crane Basin. Reconnaissance work done 100 km to the northwest in the John Day Valley, reveals that the timing of fault activity here corresponds with the fault activity in the Crane Basin. Here, the 16.1 Ma Picture Gorge basalts (Baksi, 1989) are displaced over 500 meters, forming a mid- to late-Miocene age depocenter. The 7.04 Rattlesnake tuff overlies the sediments forming a >15° angular unconformity. In between all of these large depocenters is an extensional structural fabric mid-Miocene in age. On a regional scale this zone of extensional deformation occurred at the northern tip of the Steens Mountain fault.

Following the period of distributed deformation characterized by Stage 1, a localization of deformation occurred during the late-Miocene (STAGE 2). Analyses of the Coleman Creek fault and Crane Creek fault records a drastic change in fault behavior post 9.63 Ma, as recorded



by the Devine Canyon tuff. To the east, on the Coleman Creek fault, displacement rates drastically increased by 600%. To the west, on the Crane Creek fault, the rates moderately increased by 30%.

This period of heightened activity lasted to ~7 Ma as recorded by the Drinkwater basalt. Not only were the displacement rates increased, but deformation was focused in the east. Following this period of heightened fault activity from 9.63 to ~7 Ma, rates slowed dramatically. Deformation migrated westward through the Crane Basin eventually localizing to the west

within the Harney Basin. From 9.63 Ma to the present marks Stage 2 of deformation, characterized by localization and westward migration of deformation. Unfortunately a clearer understanding of the later part of Stage 2 could not be resolved from the Crane Basin record due to the lack of a suitable stratigraphic record for this time period.

### Harney Basin Evolution

Combined, the Crane Basin and the Harney Basin possess stratigraphic columns that extend from the 16.5 Ma Steens Basalt at the base to the ~1.93 Ma Voltage basalt at the top.

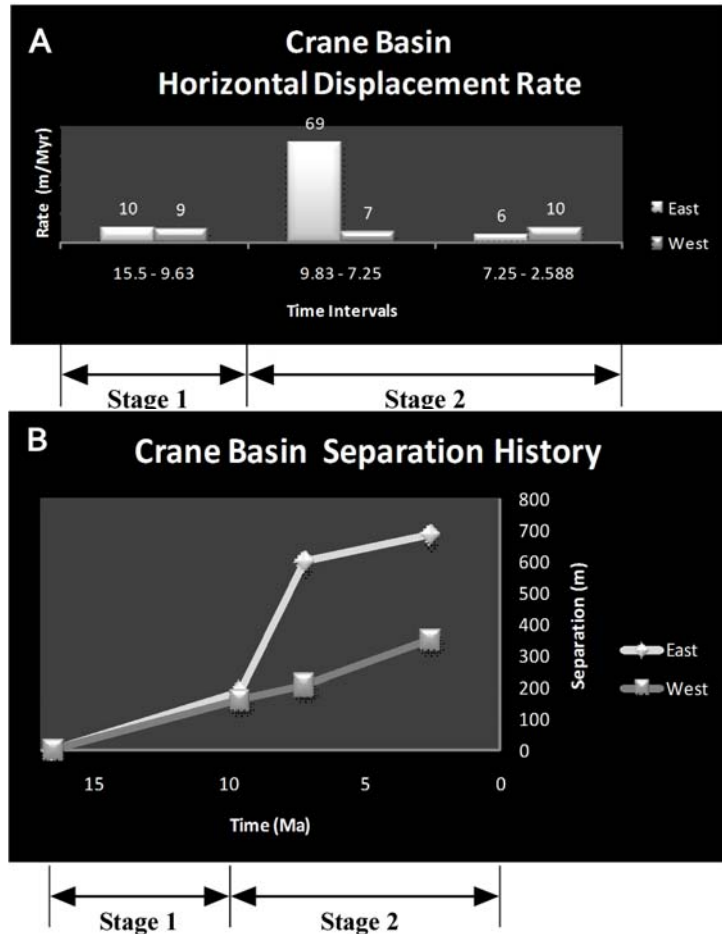


Figure 11. A) Rates of horizontal displacement for both the Eastern and Western Crane Basins. B) Separation history illustrating similar deformation for both basins during Stage 1 and then dissimilar behavior during Stage 2. Drastic spike in activity seen in east and westward migration of deformation shown as increased slope in the west basin curve.

We have discussed the extensional deformation responsible for creating the half-graben network that formed the Crane Basin depocenter. According to the domino-style basin formation model introduced by Schlische (1991), as a basin develops, the rate of volume growth controlled by subsidence decreases relative to the rate of sediment input and aggradation. This negative relationship results in a basin in which the supply of sediments exceeds the capacity of the basin. Subsidence is only resumed when older, highly rotated faults become inactive due to their inefficiency and are cross-cut by new high-angle faults. Proffett (1977) recorded three stages of faults in central Nevada, where the oldest set of faults had been successively cut by two younger sets of faults. At the termination of a fault set, when subsidence ceases, a shift from lacustrine to fluvial sedimentation occurs (Schlische, 1991) due to the effective 'filling' of the depocenter and the necessity for the input to exit.

The Crane Basin study area does not exhibit shallow normal faults that would suggest it reached this stage of development. Additionally, this study has demonstrated that deposition decreased in the Crane Basin during the Pleistocene because of the decrease in fault displacement and the rapid formation of a greater depocenter, Harney Basin, to the west. The mechanisms of the Harney Basin's formation are poorly understood, but the timing and scale of its evolution are constrained well by its strata which record regional deformation from 9.63 Ma to present.

The geology north and south of the Harney Basin, where the Devine Canyon and underlying Tts sediments are preserved, form a series of small mid-Miocene age half-grabens analogous to those found in the older Crane Basin record. This suggests that prior to 9.63 Ma the structure within the Harney Basin area was developing similarly to the Crane Basin. For reasons not clearly understood, at roughly 10 Ma, deformation in the Harney Basin greatly acceler-

ated. Subsidence greatly outpaced the rate of subsidence in the Crane Basin. This is recorded in the Western Crane Basin by the erosion and evacuation of Tdv and Tts, and the eventual aggradation of Tsts on that erosional surface. Exposed sediments of Tsts are only found in the upper part of the greater sediment column that filled the Harney Basin between the eruptions of the Devine Canyon, at 9.63 Ma, and the Drinkwater basalt at 7.25 Ma. Chronostratigraphic corollaries of the western Crane Basin Tsts can be found surrounding the Harney Basin, as mapped by Walker (1972), mapped as Tst to the north, west and south. Utilizing the dips of the southeastward dipping Devine Canyon, Prater Creek and Rattlesnake tuffs at the mouth of the Silvies River, which are roughly 6°, 3°, 1° respectively. When projected basin wards estimated depths could reach three kilometers at the center of the Harney Basin. This structural evidence suggests 3,000 meters of volcanoclastic sediment filled the Harney Basin atop bedrock of Miocene lavas of Steens Mountain and related volcanics. Five exploration wells were drilled within the Harney Basin during the mid-20<sup>th</sup> century (Table 1), four of which reached basaltic bedrock at similar depths between 750 and 1,300 meters (Houston, 2009) revealing a thick sediment column that aggraded between 9.63 and ~7 Ma. Indeed, this is a record of hyperactive deformation and subsidence that characterizes the first 2.5 Myr of Stage 2 of deformation, from 9.63 to roughly 7 Ma. Oddly, subsidence ceased as quickly as it started.

<b>Well Name</b>	<b>TD Depth (m)</b>	<b>Bedrock Depth (m)</b>	<b>Longitude</b>	<b>Latitude</b>
<i>Well 01</i>	1,160.7	914.6	-119.058	43.381
<i>Jones-Sullivan 1</i>	461.3	NA	-118.689	43.51333
<i>Fay 1</i>	1,170.1	747.0	-118.649	43.49611
<i>Weed &amp; Poteet 1</i>	1,975.6	1,137.2	-119.018	43.59696
<i>Vogler 1</i>	1,387.2	1,288.1	-118.948	43.45563
<i>Federal 1-10</i>	2,342.7	NA	-119.218	43.5941

**Table 1.**

The Harney and Crane Basins have basalt intra-basin flows that constrain the timing of base level. By utilizing these marker units and an evacuation history can be understood (Figure 12). In the Eastern Crane Basin, the Drinkwater basalt and underlying units were incised through by the paleo-river of the south fork of the Malheur River. The level of that channel is recorded by the intra-valley 1.93 Ma Voltage lava flow, which erupted in the southern Harney Basin (Camp, 2003; Greene, 1972). The approximate elevations of the Drinkwater basalt and the Voltage basalt are 1,261 and 1,044 meters, respectively. Using these elevations and the corresponding ages of the units, an incision rate can be calculated for the Crane Basin.

In the Harney Basin, three intra-basin basalt flows were utilized to represent a maximum fill level, decreased filled level, and minimum fill level. The maximum base level of the basin is recorded by the Drinkwater basalt within the western Crane Basin on the eastern margin of the Harney Basin. The Drinkwater basalt is the oldest lava flow overlying Tsts age sediments within the basin. The Crane Butte (1424m) and Windy Point Butte (1385m), which are capped by Tdw, have experienced negligible deformation since eruption which serve to represent base level at that time. The age of the Tdw basalt here has been dated to ~7 Ma by (Walker, 1979) and is petrologically similar to the Eastern Crane Basin's 7.25 Ma Drinkwater basalt. The evacuated base level of the Harney Basin is recorded by the 2.54Ma (Jordan, 2001) Wrights Point basalt flow located on the western margin of the Harney Basin. It, much like the Voltage basalt flow, filled in a paleo-depression within the greater Harney Basin to the point of flowing out of a lake, exiting eastward, downstream a distance 14km. Due to the larger extent of the Wrights Point flow, two elevations were utilized to estimate the base level of the basin at the time of its eruption, one at the head of the channeled flow (1,343m) and one at the toe (1,321m). Preserving the minimum base level of the Harney Basin is the previously described Voltage flow in the southeastern region of the Harney Basin. Numerous dates were acquired in

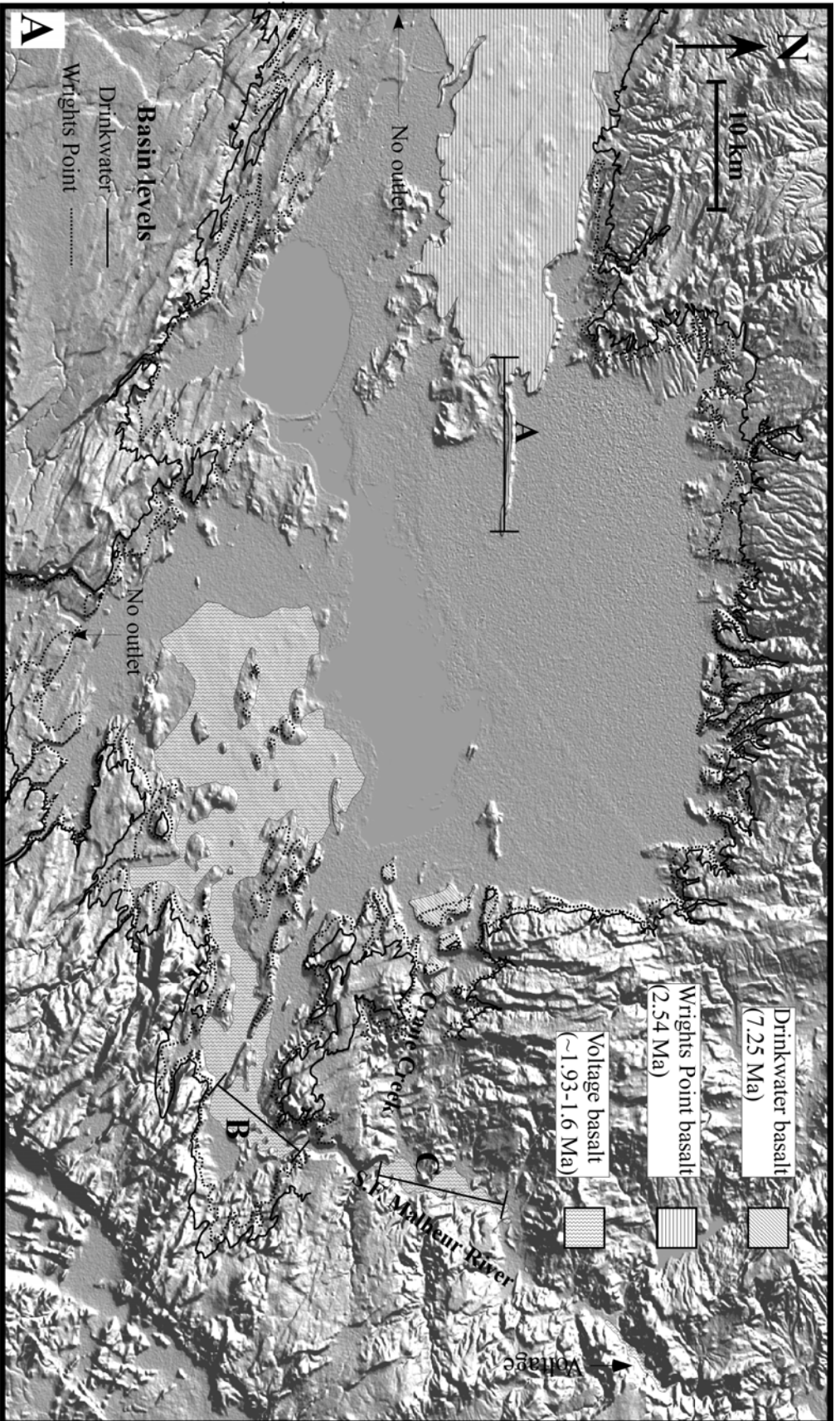


Figure 12. A) Map of southeastern Oregon displaying the three intra-basin lava flows of the Harney Basin. Extent of the Drinkwater was mapped during this study while the Wrights Point and greater Voltage basalt is shown as mapped by Walker (1972). Harney Basin base levels were estimated at three intervals during this study, recording the evacuation history of the basin. Locations of Figure 12B transects are shown.

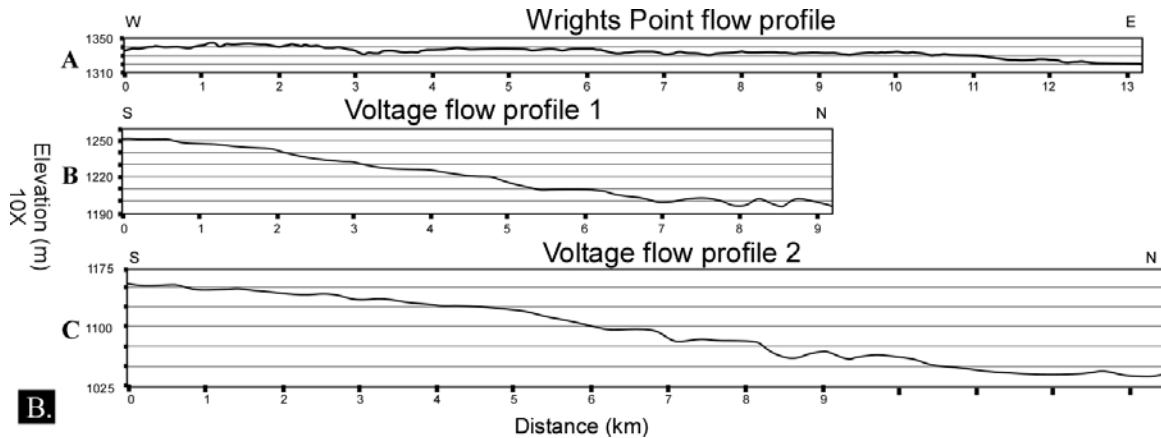


Figure 12. B) Topographic profiles of the relatively undeformed Wrights Point and Voltage lava flows. Profile A records an emptying lake system and the through-flowing nature of the Harney Basin at 2.41 Ma, serving as direct evidence of the evacuation of the Harney Basin. Profile B and C record the steep grade of the 1.93 Ma paleo-river channel of the south fork of the Malheur River which was responsible for evacuating the Harney Basin from ~7.25 to 1.93 Ma.

the area of Diamond Craters and Princeton, Oregon by Jordan (2001). In this analysis, both the dates and the multiple elevations of the flow in the region were averaged to estimate a general level and age of the basalt at the time of its eruption. In the area, an average elevation of 1,284 meters and an age of 1.5 Ma were calculated.

## Results

For the Eastern Crane Basin, an incision of ~218 meters over ~5.32 Myrs was calculated, using the Drinkwater basalt flow as the maximum base level and the Voltage basalt flow as the minimum. This amounts to an incision rate of 41 m/Myr, a relatively fast rate when compared to the Harney Basin. This rapid incision can be qualitatively observed in the South Fork Malheur River canyon. Here a paleo-canyon was formed by vertical incision through Steens Basalt bedrock by the paleo-stream responsible for incising through the Western Crane Basin stratigraphy.

In the Harney Basin, two incision rates can be calculated. The first between the ~7.25 Ma Drinkwater basalt and the 2.54 Ma Wrights Point basalt, and the second between the 2.54

Ma Wrights Point basalt and the ~1.5 Ma Voltage basalt. During the first period, 72 meters of sediment was incised, or more appropriately, evacuated from the basin over a period of 4.71 Myrs. This amounts to a rate of 15.28 m/Myr. During the second period, 48 meters of sediment was evacuated over a period of 1.04 Myrs, a rate of 46.2 m/Myrs. These rates are significantly lower than the Eastern Crane Basin rates. Intuitively, this can be justified by the drastically different geometries of the two basins; the Harney Basin is roughly 12 times the size of the Eastern Crane Basin. Less intuitively, a second interpretation can be inferred from this finding regarding the region's structural development.

The record shows that sedimentation within the Harney Basin largely ceased by roughly 7.25 Ma, which, according to the domino-style model would indicate that subsidence resulting from fault activity would also have ceased. The shift from deposition within a closed lake basin to one with an through flowing river system (the paleo-south fork of the Malheur River) also coincides with Schlische's (1991) domino-style model. If regional strain was no longer being accommodated for by brittle deformation of the crust via extensional faulting, then it must be accommodated for by another mechanism.

Mentioned previously, the correlations between fault events and volcanic events have been found numerous times in the region. From 7.8 to 7.5 Ma the greatest of three peaks in HLP basaltic volcanism occurred (Jordan, 2002). The two following periods of peak activity were at 5.9 to 5.3 Ma and 3 to 2 Ma (Jordan, 2002). It is possible that the last 7 Myr of accumulated strain at the Northwestern margin of the Basin and Range Province has been accommodated for by dual forms of deformation; brittle faulting represented by the development of the Brothers Fault Zone and magmatically by the basalt dike injection across the entire High Lava Plains. Evidence suggests that the en echelon faults of the Brothers Fault Zone formed from ~7

Ma to 5 Ma (Iademarco, 2009; Trench, 2008). The Brothers Fault Zone faults largely dip north-east, down-dropping the Harney Basin and the region north of the lineament down relative to the High Lava Plains. High Lava Plains Basalt volcanism peaked post ~7.6 Ma, specifically in an episodic manner, across the entirety of the Brothers Fault Zone and High Lava Plains trend. Analogously, basaltic dikes have been demonstrated to extensively accommodate extension in the Snake River Plain, up to 20% in the eastern Snake River Plain, immediately east of the Crane Basin study area (Rodgers, 2002).

## **Conclusion**

Southeastern Oregon is dominated by moderate (>100m) topographic escarpments that are the result of young (<10 Ma) Basin and Range extensional tectonics. Previous work has identified that extension migrated northward into this region between 45 Ma and 15 Ma from central Nevada (Christiansen, 1992; Colgan, 2006; Dickinson, 2002; Lerch, 2008) (Fig. 13). Separating the >15 Ma well-developed region from the <10 Ma poorly developed region of the Basin and Range is a distinct boundary. At its northern limit in southeast Oregon, the boundary is expressed as the Steens Mountain fault, and continues south as a series of large-displacement (>500m) normal faults, eventually linking up with the Carlin Sink in northwest Nevada and onto the Walker Lane in eastern California. During the mid-Miocene, magmatic and fault activity was heightened at the northern tip of this boundary. Magmatically this was expressed as the eruptions of the McDermitt Caldera and Steens Mountain flood basalt. Structurally this expressed as the northward propagation of the Steens Mountain fault, at whose northern tip developed a broad region of distributed deformation responsible for forming the Oregon-Idaho Graben, the Crane Basin, the John Day Basin and additional extensional fault fabric in between these depocenters from ~15.5 Ma to 9.63 Ma (STAGE 1).



In the Crane Basin, this period of development characterized Stage 1 of the basin's history. During Stage 1, organization of the basin's north - south trending normal faults formed a series of interconnected half-grabens whose subsidence was adequate to form a depocenter. Fault histories in the eastern and western parts of the basin were recorded on the Coleman Creek and Crane Creek faults, respectively. Well-constrained  $^{40}\text{Ar}/^{39}\text{Ar}$  ages on volcanic marker beds within the basin's stratigraphy allowed for a temporal record to be extrapolated. During the Stage-1, similar percentages of total fault displacement occurred in both the east and west portions of the Crane Basin, demonstrating that that strain was evenly distributed across the region. The faulting history following 9.63 Ma demonstrates that that strain was localized and that the resulting deformation was episodic in nature.

Post 9.63 Ma deformation in the Crane Basin characterizes Stage 2 of the basin's development. During Stage 2, deformation was not broadly distributed across the entire fault network formed in the previous ~6 Myr, but rather was localized to the dominant structures. Analyses reveal the post ~10 Ma episodic nature of displacement upon the Crane Basin faults and the western migration of deformation. Displacement rates increased by ~600% on the Coleman Creek fault and by 30% on the Crane Creek fault during the period between 9.63 Ma and 7.25 Ma. Occurring during this same time was the rapid subsidence of the Harney Basin. Both the events in the Crane and Harney Basin temporally coincide with the most voluminous episode of High Lava Plains volcanism. Suggesting that an intimate link exists between the two mechanisms, brittle faulting and magmatism, for accommodating extensional strain during the development of the immature northwest margin of the Basin and Range Province. Post 7.25 Ma the activity upon Crane Basin faults decreased.

The Crane Basin depocenter records the temporal and structural development of the northwestern margin of the Basin and Range Province. The boundary evolved from a region of distributed fault deformation to one of localized deformation. Structurally the region had a history that closely correlated to regional magmatic activity, both spatially and temporally, indicating that a strong link exists between the initial stages of Basin and Range structural development and accompanying magmatic activity.

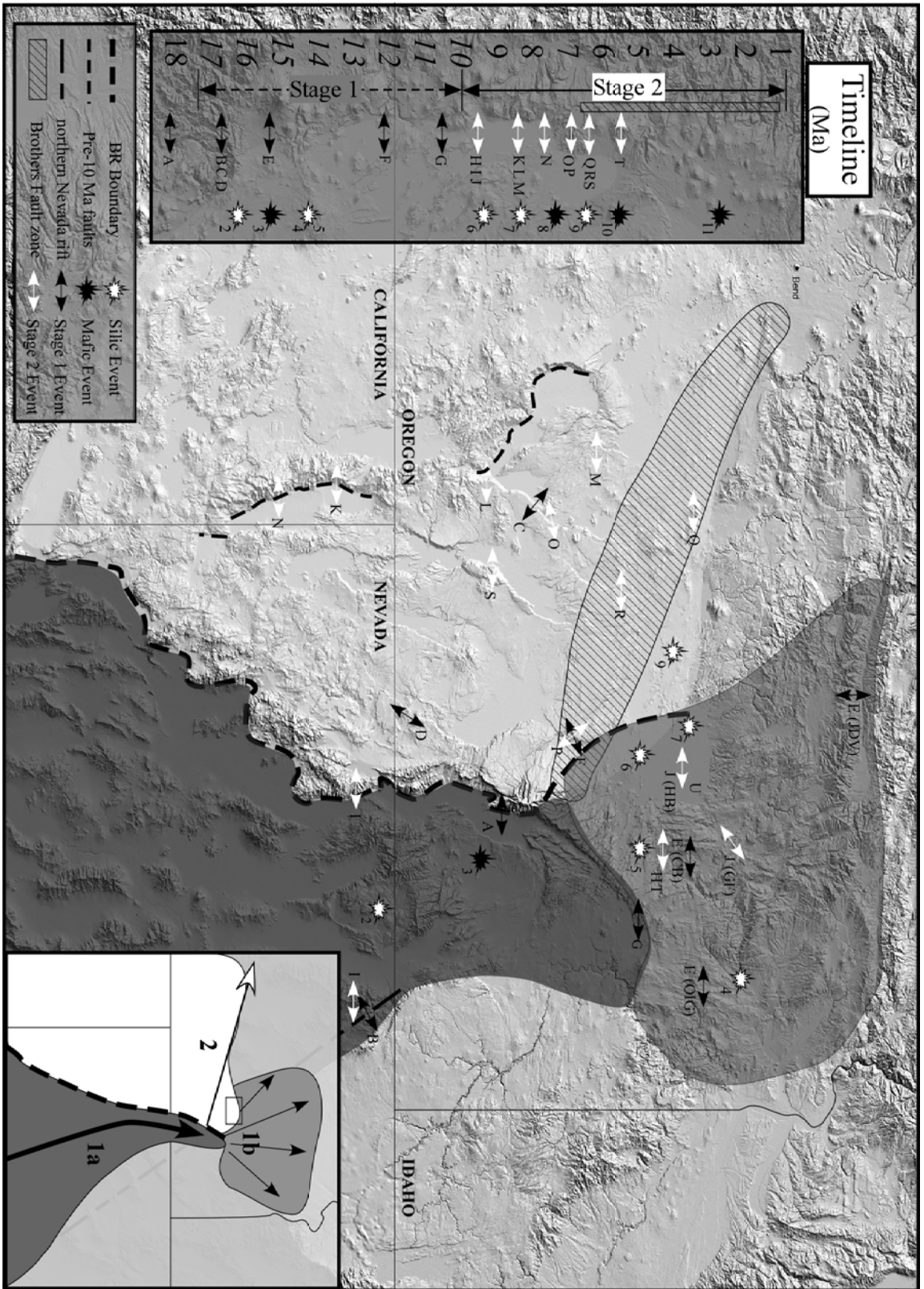


Figure 13 (Previous Page). **DEM of northwestern margin of the Basin and Range Province with chronologic sequence of volcanic (numbers) and extensional (letters) events plotted on a timeline with the corresponding Stage 1 and 2 of Crane Basin development. Well developed extensional fabric of the Basin and Range (shaded dark gray) migrated northwestwards into SE Oregon during the mid-Miocene (~18 – 16 Ma) forming a NE-SW trending boundary (heavy dashed line). STAGE 1: Focus of deformation at the northern tip of the Steens Mountain fault resulted in broad, distributed tecto-magmatic deformation from ~15.5 – 9.63 Ma (shaded light gray). STAGE 2: Localized deformation west of the boundary at the northern limit, marked by heightened episodes of both tectonic and magmatic activity. Deformation migrates westwards away from the boundary developing the youngest manifestation of Basin and Range extensional fabric (shaded white). (*Evidence from this study is italicized*)**

**A:** >20 degree angular unconformity at the base of the Steens basalt on the southern escarpment of the Steens mountain, recording significant displacement and rotation of the footwall black prior to 16.5 Ma (Langer, 1991; Minor, 1987); **B:** Development of the northern Nevada rift between 17 & 14 Ma (Zoback, 1994); **C:** Existence of fault related topography prior to the 16.5 Ma Steens Mountain Basalt at the Abert Rim (Scarberry, 2009); **D:** Development of the Hawks Valley graben from ~16 – 10 Ma (Legge, 1988; Maloney, 1961; Scarberry, 2009); **E:** Initiation of distributed deformation at the northern tip of the Steens mountain fault manifested by deformation forming the Oregon-Idaho Graben (15.5 – 10.3 Ma) (Cummings, 2000), *Crane Basin (~15.5 – 10 Ma)*, John Day Valley (post 15 – 7 Ma) and interstitial N-S trending extensional fault fabric; **F:** Development of NW trending faults on Sheepshead Mountain ~12-9 Ma (Sherrod, 1988); **G:** ~10 Ma fault activity on NNE trending faults at Duck Buttes (Johnson, 2000); **H:** *Crane Basin shift in fault behavior, localization of deformation and heightened activity ~10-7Ma*; **I:** Post 10 Ma extension in the Santa Rosa-Pine Forest (Colgan, 2006); **J:** Rapid subsidence of the Harney Basin post 9.63 Ma, ceasing by ~7 Ma, similar estimated timing of Grasshopper Flat subsidence (Johnson J. A., 1998); **K:** Uplift of the Warney Range upon the Summer Lake Fault initiating between 8 & 4 Ma (Carmichael, 2006); **L:** Activation of faults proximal to Drake Peak along the southern Abert Rim prior to 9-7 Ma (Scarberry, 2009; Wells, 1980); **M:** Rotation of paleomagnetic indicators in Devine Canyon tuff not Rattlesnake (Stimac, 1992); **N:** NW trending faults formed and successively cut by NE trending Abert Rim between 8.9 & 7.5 Ma (Scarberry, 2009); **O:** Documented similar vertical slip rates on Summer Lake Fault between modern paleoseismic evidence and estimated long term rates initiating ~14 – 8 Ma (Personius, 2009); **P:** NW trending faults of Sheepshead Mountain cut NE at ~7 Ma (Sherrod, 1988); **Q:** Apparent westward progressive faulting of fabric surrounding Hampton Butte between ~7 & 5 Ma (ideamarco, 2009); **R:** Fault linkage of NE faults to NW Brothers Fault zone at ~7 & 5 Ma peak in activity (Trench and Meigs, 2008); **S:** No angular discordance documented at Poker Jim Ridge suggesting no extension prior to 7 Ma (Hart, 1982; Scarberry, 2009); **T:** *Drastic decrease of fault activity post ~7 Ma in Crane Basin*; **U:** *Post 7 Ma ceasing of Harney Basin subsidence and localization of faulting to its southern Brothers Fault zone boundary*

**1:** Organization and development of the northern Nevada rift dike system between 17 & 14

Ma (Zoback, 1994); **2**: Eruption of the McDermitt caldera ~17-15 Ma and initiation of “related” Yellowstone magmatism (Colgan, 2004); **3**: Eruption of the Steens Mountain flood basalt at ~16.5 Ma (Swisher, 1990), the initial flow of the larger Columbia River basalts; **4**: Syntectonic magmatism within the Oregon-Idaho Graben ~15.5 – 10.3 Ma (Cummings, 2000); **5**: *Syntectonic rhyodacitic magmatism within the Crane Basin* ~15.5 – 10; **6**: Devine Canyon ash-flow tuff 9.63 Ma (Ford, 2009); **7**: Prater Creek ash-flow tuff 8.41 Ma (Streck et al., 1999); **8**: First, and greatest peak in High Lava Plains basalt volcanism ~7.8 – 7.5 Ma (Jordan, 2004a); **9**: Rattlesnake ash-flow tuff 7.04 Ma (Streck and Grunder, 1995); **10**: Second peak in HLP basaltic volcanism ~5.9 – 5.3 Ma (Jordan, 2004a); **11**: Third peak in HLP basaltic volcanism ~3 – 2 Ma (Jordan, 2004a).

**Inset:** Generalized sequence of events; 1a: Northern migration of tectono-magmatic deformation front forming western boundary (bold dashed line) of the highly extended Basin and Range (dark gray); 1b: distributed deformation at the northern tip of developed Basin and Range (light gray); 2: Deformation localized to a general E-W trend from the northern tip of the Steens Mountain fault, episodic heightened deformation migrating westward from boundary (white). Black rectangle outlines Crane Basin study area.

## **Crane School District Field Trip**

On August 27, 2008, a field trip was led by Mr. Charles Steeves and me for two science classes from the Crane School District with approximately 45 students total. It was arranged with the district's superintendent, Mrs. Pat Sharp, through my liaison Mr. Chuck Steeves. The goal of the trip was to spend a half day learning about the geologic history of the region surrounding the town of Crane, Oregon and teaching the students about the rocks in the area in which they live.

The field trip started with an informal Powerpoint presentation. The focus of the 30-minute talk was to use pictures and videos of rock types in the area and their respective depositional environments to familiarize the students with. Through direct visualization of geology, we were able to successfully bring context and understanding of topics to both levels of students, 3<sup>rd</sup> and 8<sup>th</sup> grade science classes. I received direct feedback from students, who were very interested in the topic and asked numerous of questions. I was also complimented by Mr. Steeves and superintendent Sharp on the quality and ease of understanding displayed in the talk.

Mr. Steeves arranged for a school district bus to be available for transportation. I received overly willing permission from local, private landowners to access land and outcrops. Due to the young age of the field trip and time constraints, the trip was limited to the immediate region around Crane, Oregon. While in transit I gave a general overview of the rocks along the road, how they formed and their volcanic history. I also illustrated the paleo-environments of the region and the animals that once existed there, a precursor to fossils I had located previously in an outcrop that I intended to let the students find. We hiked along the railroad grade from the base of SS 7 to the upper part of SS 1. We discussed basic rock observations, identi-

fied if they were igneous or sedimentary, explained their colors, and discussed how the rocks might have formed. The majority of students were intrigued and directly participated in discussion but due to the large size of the group and range in age some students became preoccupied with finding fossils.

At two locations along the railroad cut were vertebrate fossils that were relatively well exposed. Students eventually found both locales and discovered three fossils. One student even successfully identified a normal fault. Following the cataloging of fossils and photo documentation, the specimens were donated to the school district to be put on display in the science room.

Overall, the response to the field trip by students, school staff and the community was extremely positive. Dr. Andrew Meigs offered to lead future trips or talks if the school district would like to have similar activities in the future.



Figure 14. Images taken during Crane School District field trip in the Crane Basin field area. (Left) Students are locating late-Miocene age vertebrate fossils within a Tsts outcrop. (Right) Student in the white hat next to instructor (me) identified a normal fault that offset beds of tuffaceous sandstone. He explained his observation and rationale to his fellow participants demonstrating his retaining of knowledge learned during the morning lecture .

Bibliography



## Bibliography

- Anderson, R. E., M.L. Zoback, G.A. Thompson, 1983, Implications of selected subsurface data on the structural form and evolution of some basins in the northern Basin and Range province, Nevada and Utah: Geological Society of America Bulletin, v. 94, p. 1055-1072.
- Baksi, A. K., 1989, Reevaluation of the timing and duration of extrusion of the Imnaha, Picture Gorge, and Grande Ronde Basalts, Columbia River Basalt Group: Volcanism and Tectonism in the Columbia River Flood-Basalt Province, v. Special Paper Geological Society of America 239, p. 105-111.
- Camp, V. E., 2009, Personal communication discussing the Dinner Creek ash-flow tuff in the Crane Basin, *in* Milliard, J. B., ed.: Corvallis, OR.
- Camp, V. E., Martin, R.E., Hanson, W.E. , 2003, Genesis of flood basalts and Basin and Range volcanic rocks from Steens Mountain to the Malheur River Gorge, Oregon: GSA Bulletin, v. 115, no. 1, p. 105-128.
- Carmichael, I. S. E., R. A. Lange, C. M. Hall, P. R. Renne, 2006, Faulted and toltd Pliocene olivine-tholeiite lavas near Alturas, NE California, and their bearing on the uplift of the Warner Range: Geological Society of American Bulletin, v. 118, no. 9/10, p. 1196-1211.
- Carlson, R., 2009, Virginia Gap Basalt Geochemistry: Washington, DC, Department of Terrestrial Magnetism, Carnegie Institution for Washington.
- Carlson, R. W. a. H., 1987, Crustal genesis on the Oregon Plateau: Journal of Geophysical Research, v. 92, p. 6191-6206.
- Carlson, R. W. a. H., W. K., 1988, Flood basalt volcanism in the northwestern United States, Continental flood basalts, Macdougall, J. D.: Dordrecht, Netherlands, Kluwer Academic Publishers.
- Christiansen, R. L., R.S. Yeats, S.A. Graham, W.A. Niem, A.R. Niem, P.D. Snively Jr., 1992, Post-Laramide geology of the U.S. Cordilleran region: The Geology of North America, v. G-3, The Cordilleran Orogen: Conterminous U.S., p. 261-406.
- Colgan, J. P., T.A. Dumitru, P.W. Reiners, J.L. Wooden, E.L. Miller, 2006, Cenozoic tectonic evolution of the Basin and Range Province in Northwestern Nevada: American Journal of Science, v. 306, no. October, p. 616-654.
- Colgan, J. P., T. A. Dumitru, E. L. Miller, 2004, Diachroneity of Basin and Range extension and Yellowstone hotspot volcanism in northwestern Nevada: Geology: Geological Society of America, v. 32, p. 121-124.

- Compton, R. R., 1985, *Geology in the field*.
- Cummings, M. L., J. G. Evans, M. L. Ferns and K. R. Lees, 2000, Stratigraphic and structural evolution of the middle Miocene synvolcanic Oregon-Idaho graben: *Geological Society of America Bulletin*, v. 112, p. 668-682.
- Dickinson, W. R., 2002, The Basin and Range Province as a Composite Extensional Domain: *The International Geology Review*, v. 44, p. 1-39.
- Fiebelkorn, R. B., G. W. Walker, N. S. MacLeod, E. H. McKee, J. G. Smith, 1983, Index to K-Ar Determinations for the State of Oregon: *Isochron/West*, no. 37, p. 3-60.
- Ford, M., et al., 2009, PhD Dissertation in preparation: Oregon State University.
- Fremd, T., 2008, Personal Communication regarding Crane Basin vertebrate fossils, *in* Milliard, J. B., ed.: Kimberly, OR.
- Goldfinger, C., L.D. Kulm, R.S. Yeats, L. McNeill, C. Hummon, 1997 Oblique strike-slip faulting of the central Cascadia submarine forearc: *Journal of Geophysical Research*, v. Solid Earth, no. 102 (B4), p. 8217-8243.
- Greene, R. C., G.W. Walker, R. E. Corcoran, 1972, *Geologic Map of the Burns Quadrangle, Oregon*, scale 1:250,000.
- Gutmanis, J. C., 1989, Wrench faults, pull-apart basins, and volcanism in Central Oregon - a new tectonic model base on image interpretation: *Geologic Journal*, v. 24, no. 3, p. 183-192.
- Haddock, G. H., 1967, *The Dinner Creek Ashflow Welded Tuff of the Malheur Gorge area: University of Oregon*.
- Hart, W. K., S. A. Metzman, 1982, K-Ar ages of basalts from southcentral and southeastern Oregon: *Isochron/West*, v. 33, p. 23-26.
- Houston, R., 2009, *Exploration Oil and Gas Well Logs: Albany, State of Oregon, Department of Geology and Mineral Industries*.
- Iademarco, M. J., 2009, *Volcanism and Faulting along the Northern Margin of Oregon's High Lava Plains: Hampton Butte to Dry Mountain: Oregon State University*, 158 p.
- Johnson D. M., P. R. H., and R. M. Conrey, 1999, XRF Analysis of Rocks and Minerals for Major and Trace Elements on a Single Low Dilution Li-tetraborate Fused Bead: *Joint Committee on Powder Diffraction Standards*, p. 843 - 867.
- Johnson, J. A., A.L. Grunder, 2000, The making of intermediate composition magma in a bimodal suite: Duck Butte Eruptive Center, Oregon, USA: *Journal of Volcanology and Geochemical Research*, v. 95, p. 175-195.

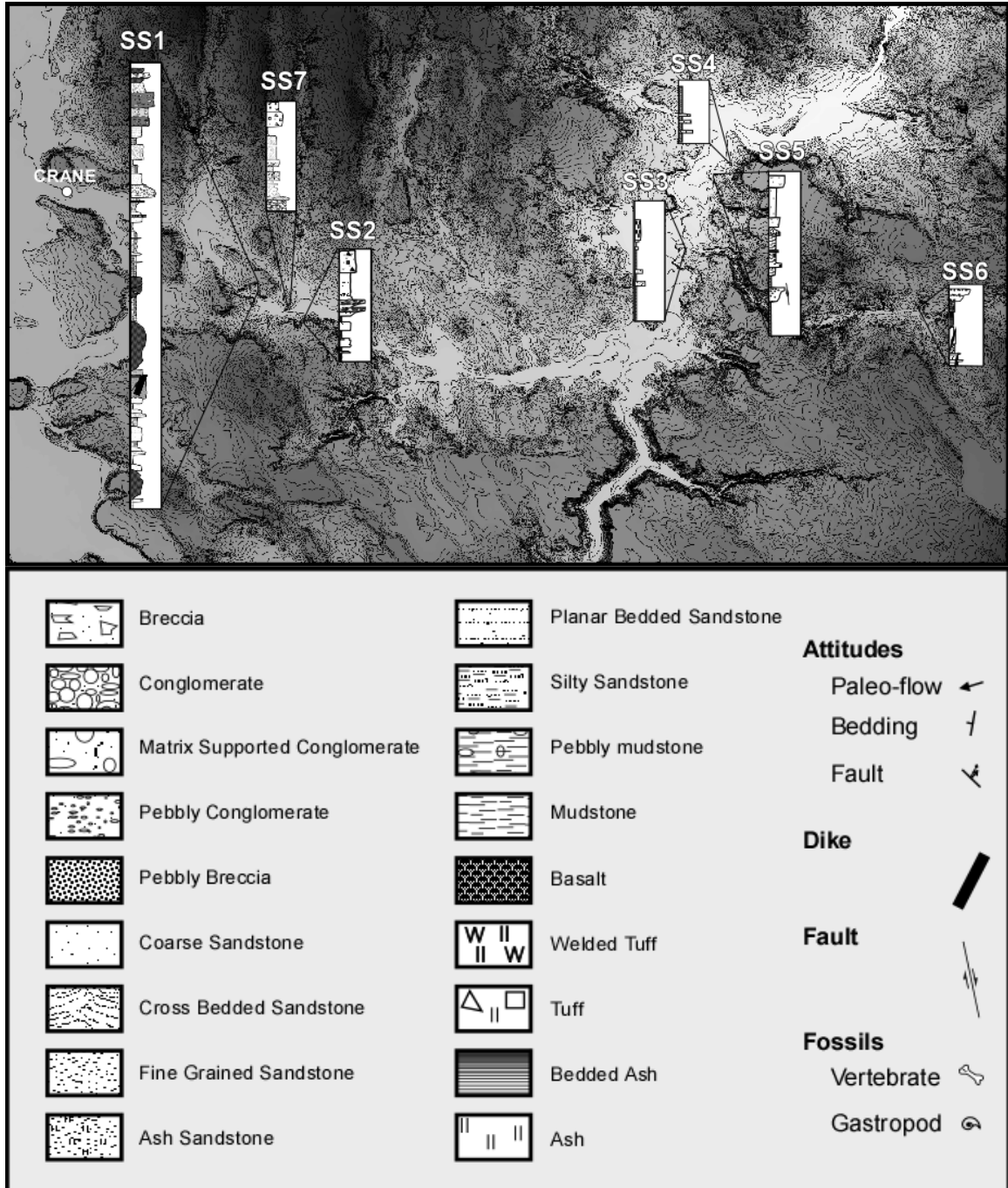
- Johnson, J. A., Hopper P.R., Hawkesworth C.J., Binger G.B., 1998, Geologic Map of the Stemler Ridge Quadrangle, Malheur County, Southeastern Oregon: U.S. Geological Survey.
- Jordan, B. T., 2001, Basaltic Volcanism and Tectonics of the High Lava Plains, Southeastern Oregon: Oregon State University, 218 p.
- Jordan, B. T., Streck, M.J., and A. L. Grunder, 2002, Bimodal volcanism and tectonism of the High Lava Plains, Oregon: Oregon Department of Geology and Mineral Industries Special Paper, p. 23-46.
- Jordan, B. T. a. A. L. G., R.A. Duncan, A.L. Deino, 2004, Geochronology of age-progressive volcanism of the Oregon High Lava Plains: Implications for the plume interpretation of Yellowstone: *Journal of Geophysical Research*, v. 109, no. B10202, p. 1-19.
- Knaack, C., S. Cornelius, P. R. Hooper, 1994, Trace element analysis of rocks and minerals by ICP-MS: Open File Report, Department of Geology, Washington State University.
- Langer, V. W., 1991, Geology and petrologic evolution of silicic and intermediate volcanic rocks underneath Steens Mountain basalt, SE Oregon: Queen's University, 109 p.
- Lavallée, Y., S.L. de Silva, G. Salas, J.M. Barnes, 2009, Structural control on volcanism at the Ubina, Huaynaputina, and Ticsani Volcanic Group (UHTVG), southern Peru: *Journal of Volcanology and Geothermal Research*, v. 186, p. 253-264.
- Legge, P. W., 1988, The bimodal basalt-rhyolite association west of and adjacent to the Pueblo Mountains, southeastern Oregon: Miami University of Ohio.
- Lerch, D. W., E. Miller, M. McWilliams, J. Colgan, 2008, Tectonic and magmatic evolution of the northwestern Basin and Range and its transition to unextended volcanic plateaus: Black Rock Range, Nevada: *Geological Society of America Bulletin*, v. 120, p. 300-311.
- Maloney, N. J., 1961, Geology of the Eastern Part Beaty Butte Four Quadrangle, Oregon: Oregon State University, 88 p.
- McDonough, W. F., and S. -s. Sun, 1995, The composition of the Earth: *Chemical Geology*, v. 120, no. 3-4, p. 223-253.
- Meigs, A., P.R. Carlson, J. Donnelly-Nolan, A. Grunder, B. Hart, M. Fouch, K. Scarberry, T. Grove, B. Jordan, M. Streck, M. Ford, M. Iademarco, J. Milliard, D. Trench, 2009, Field Trip Guide: Geological and Geophysical Perspectives on the Magmatic and Tectonic Development of the Northwest Basin and Range, *in* Sherrod, S., ed., 2009 Geological Society of America Annual Conference: Portland, OR, Geological Society of America.
- Minor, S. A. D. P., L.E., Esparza, T. J. Peters, 1987, Geologic map of the High Steens and Little Blitzen Gorge wilderness study areas, Harney County, Oregon.

- Nash, B. P., M. E. Perkins, J. N. Christensen, D-C Lee & A. N. Halliday, 2006, The Yellowstone hotspot in space and time: Nd and Hf isotopes in silicic magmas: *Earth and Planetary Science Letters*, v. 247, no. 1-2, p. 143-156.
- Newton, V. C., Jr., R.E. Corcoran, and R.J. Deacon 1962, *Petroleum Exploration in Oregon: State of Oregon: Department of Geology and Mineral Industries*, v. Miscellaneous Paper no. 9, p. 1-7.
- Pezzopane, S. K., R. Weldon II, 1993, Tectonic Role of Active Faulting in Central Oregon: *Tectonics*, v. 12, no. No 5, p. 1140-1169.
- Personius, S. F. A. J. C., M. N. Machette, S. A. Mahan, D. J. Lidke, 2009, Moderate rates of late Quaternary slip along the northwestern margin of the Basin and Range Province, Surprise Valley fault, northeastern California: *Journal of Geophysical Research*, v. 114, no. B09405, p. 1017.
- Proffett, J. M. J., 1977, Cenozoic geology of the Yerington district, Nevada, and implications for the nature and origin of Basin and Range faulting: *Geological Society of America Bulletin*, v. 88, p. 247-266.
- Renne, P. R., A. L. Deino, R. C. Waler, B. D. Turrin, C. C. Swicher, T. A. Becker, G. H. Curis, W. D. Sharp, and A. R. Jaouni, 1994, Intercalibration of astronomical and radioisotopic time: *Geology*, v. 22, p. 783-786.
- Rodgers, D. W., H.T. Ore, R.T. Bobo, N. McQuarrie, N. Zentner, 2002, Extension and Subsidence of the Eastern Snake River Plain: *Idaho Geological Survey Bulletin: Tectonic and Magmatic Evolution of the Snake River Plain*, v. 30, p. 121-155.
- Rollinson, H. R., 1993, *Using Geochemical Data: evaluation, presentation, interpretation: Essex, England, Pearson Education Limited*.
- Scarberry, K., A. J. Meigs, A. L. Grunder, 2009, Faulting in a propagating continental rift: Insight from the late Miocene structural development of the Abert Rim fault, southern Oregon, USA: *Tectonophysics*, p. 16.
- Scarberry, K., A. J. Meigs, and A. L. Grunder, 2008, Faulting in a propagating continental rift: insight from the late Miocene structural development of the Abert Rim fault, southern Oregon, USA: In submission to *Tectonophysics*.
- Schlische, R. W., 1991, Half-graben basin filling models: New constraints on continental extensional basin development: *Basin Research*, v. 3, p. 123-141.
- Schlische, R. W., 1994, Rifting in eastern North America: *Virginia Explorer*, v. 10, p. 20-23.

- Schlumberger, 1952, Harney County Oil and Gas wells, *in* Oregon Department of Geology and Mineral Industries: The Oil, G. G., ed.: Albany, p. Various communications and well site information, mudlogs, resistivity, etc.
- Sherrod, D. R., A. Griscom, R. L. Turner, S. A. Minor, D. E. Graham, A. R. Buehler, 1988, Mineral resources of the Sheephead Mountains, Wildcat Canyon, and Table Mountain Wilderness Study Areas, Malheur and Harney Counties, Oregon, *in* Survey, U. S. G., ed.
- Stimac, J. P., R. J. Weldon, 1992, Paleomagnetism and tectonic rotation of the Rattlesnake Ash-flow tuff, southern Oregon [Thesis thesis]: University of Oregon.
- Streck, M. J., A. L. Grunder, 1995, Crystallization and welding variations in a widespread ignimbrite sheet, the Rattlesnake Tuff, eastern Oregon, USA: *Bulletin of Volcanology*, v. 57, no. 3, p. 18.
- Streck, M. J., Grunder, A., 1999a, Enrichment of basalt and mixing of dacite in the rootzone of a large rhyolite chamber: inclusions and pumices from the Rattlesnake Tuff, Oregon: *Contributions to Mineralogy and Petrology*, v. 136, p. 193-212.
- Streck, M. J., J. A. Johnson, A. L. Grunder, 1999b, Field guide to the Rattlesnake Tuff and High Lava Plains near Burns, Oregon, *in* Neuendorf, K. K. E., ed., GAS, Cordilleran Section 1996 meeting: Portland, OR, Oregon Department of Geology and Mineral Industries, p. 65-76.
- Swisher, C. C., J.A. Ach, W.K. Hart, 1990, Laser fusion  $^{40}\text{Ar}/^{39}\text{Ar}$  dating of the type Steens Mountain Basalt, southeastern Oregon and the age of the Steens geomagnetic polarity transition: *EOS [Transactions, American Geophysical Union]*, v. 71, p. 1296.
- Trench, D. A. M., 2008, The Termination Of The Northwest Basin And Range Into A Northwest Trending Extensional Fault System: *Eos Trans. AGU*, v. 88, no. 52, p. T31C-0593.
- Vallier, T. L., 1995, Petrology of pre-Tertiary igneous rocks in the Blue Mountains region of Oregon, Idaho, and Washington: Implications for the geologic evolution of a complex island arc, *in* Survey, U. S. G., ed., p. 125-209.
- Walker, G. M., N.S. MacLeod, P. Ernest, M. Newman, D. Garcia, J. Goodman, E. Myers, 1991, *Geologic Map of Oregon*: United States Geological Survey.
- Walker, G. W., 1979, Revisions of the Cenozoic Stratigraphy of Harney Basin, Southeastern Oregon: United States Geological Survey.
- Walker, J. D. G., J.W., 2009, *Geologic Time Scale*, Geological Society of America.
- Wallace, R. E., 1979, Earthquakes and the prefractured state of the western part of the North American continent, *in* Proceedings of the International Research Conference on Intra-Continental Earthquakes, Ohrid, Yugoslavia.

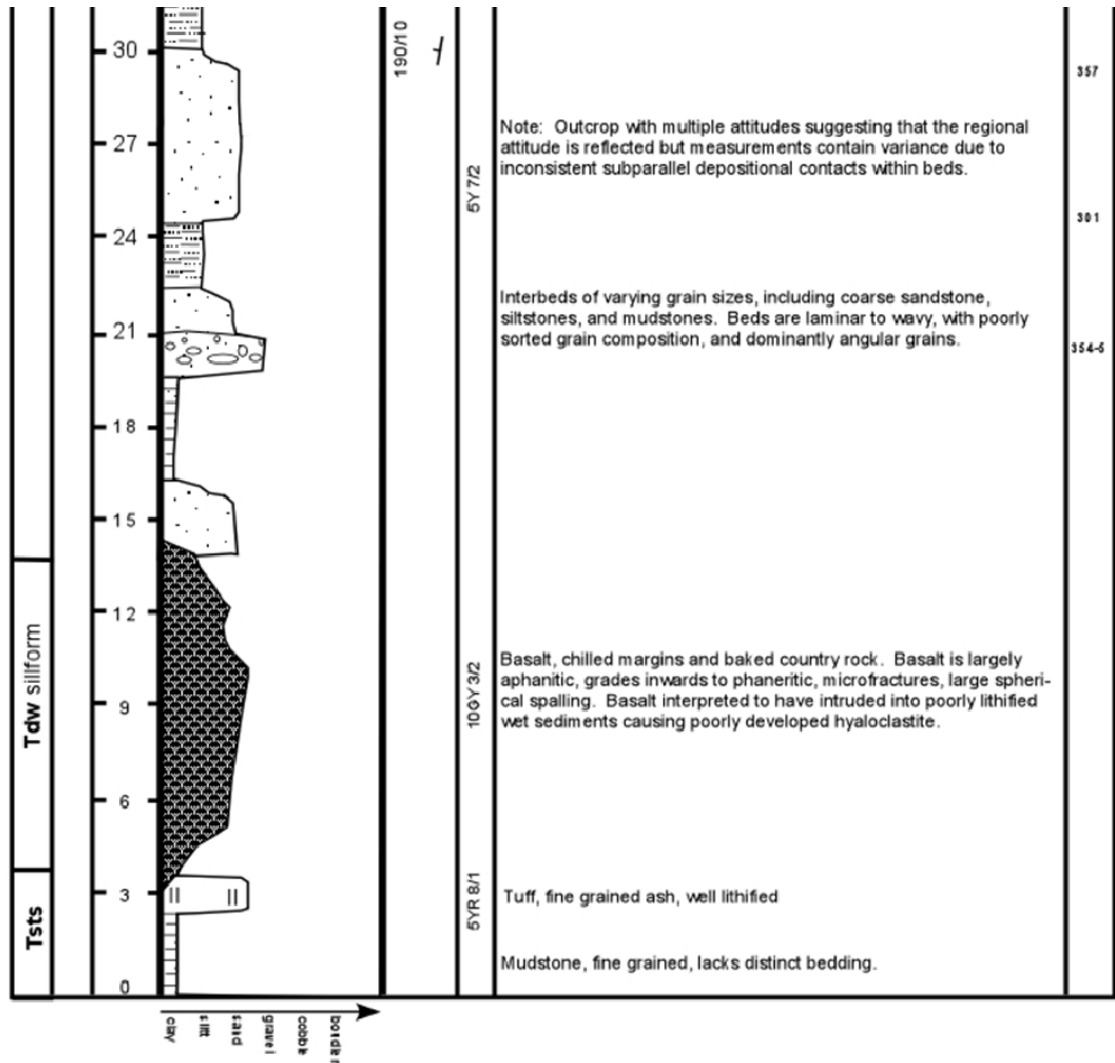
- Wells, R. E., 1980, Drake Peak - a structurally complex rhyolite center in southeastern Oregon, *in* *Survey*, U. S. G., ed., p. 16.
- Wernicke, B. P. a. B. C. B., 1982, Modes of extensional tectonics: *Journal of Structural Geology*, v. 4, p. 105-115.
- Zoback, M. L., E. H. McKee, R. J. Blakely, G. A. Thompson, 1994, The northern Nevada rift: Regional tectono-magmatic relations and middle Miocene stress direction: *Geological Society of America Bulletin*, v. 106, p. 37`-382.

## Appendices

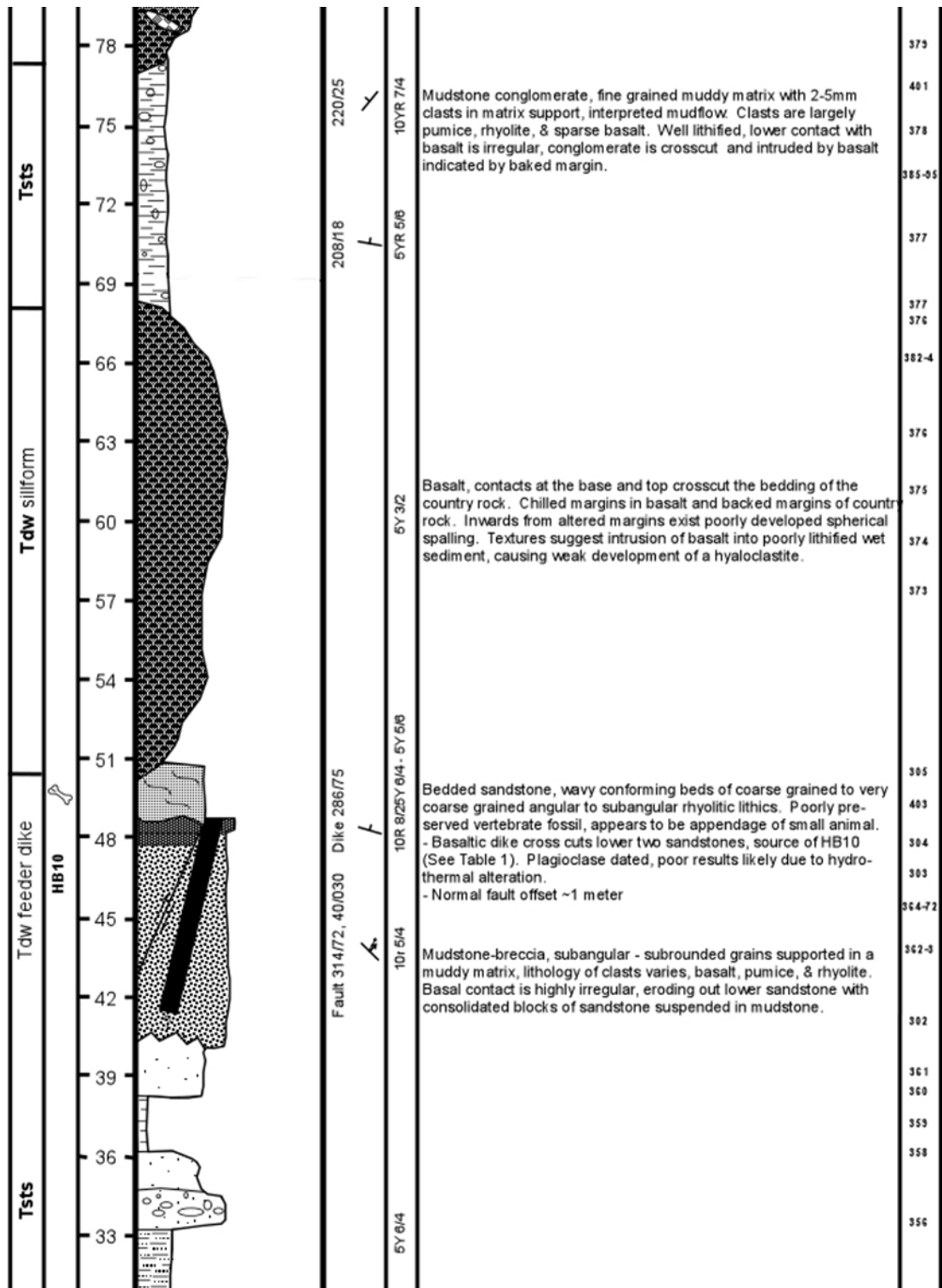


Appendix Figure 1. Stratigraphic section location map (Top) and the key to stratigraphic sections (Bottom). The geologic record documented in stratigraphic sections 1-7 represent the full range of depositional environments in the Crane Basin, from mass wasting at the margins, to fluvial at the intermediate parts of the basin, to lacustrine and playa at the center. The model used for the stratigraphic columns was adapted from Compton (1985).

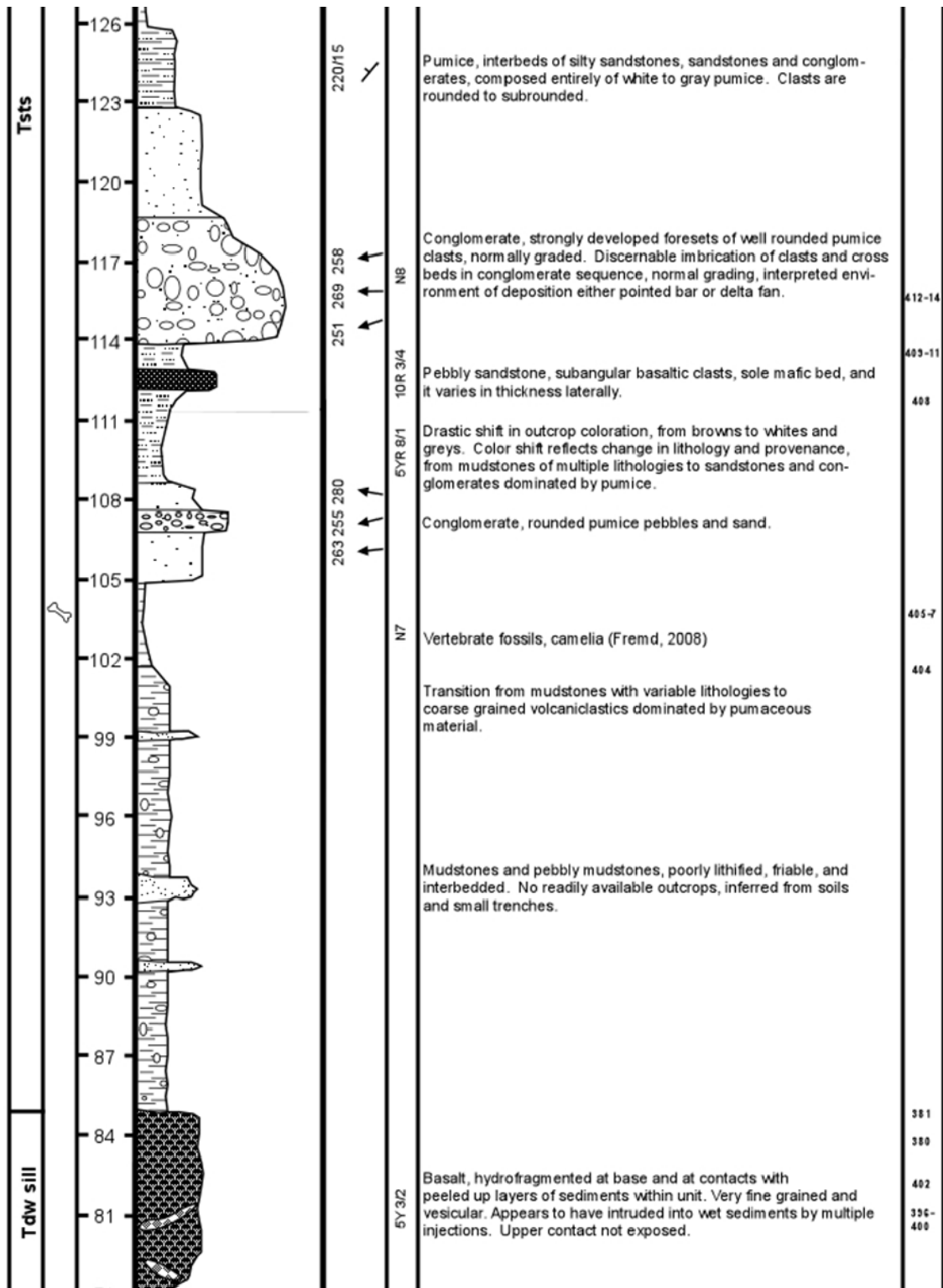







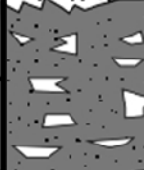

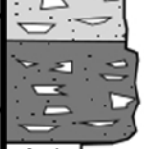




Appendix Figure 2. Stratigraphic Section 1 of Tsts in the Western Crane Basin. The measured section illustrates the fluvial and lacustrine depositional environments that existed during the filling of the Harney Basin. Hyaloclastitic and altered nature of basalt intrusions and flows further support a very wet environment and sediment column at the time of the Drinkwater eruption. The thickness of the section, though only a proxy for Tsts deposition in the greater Harney Basin, indicates a high deposition rate during the relatively short (~3 Myr) time period of Harney Basin subsidence and infilling.



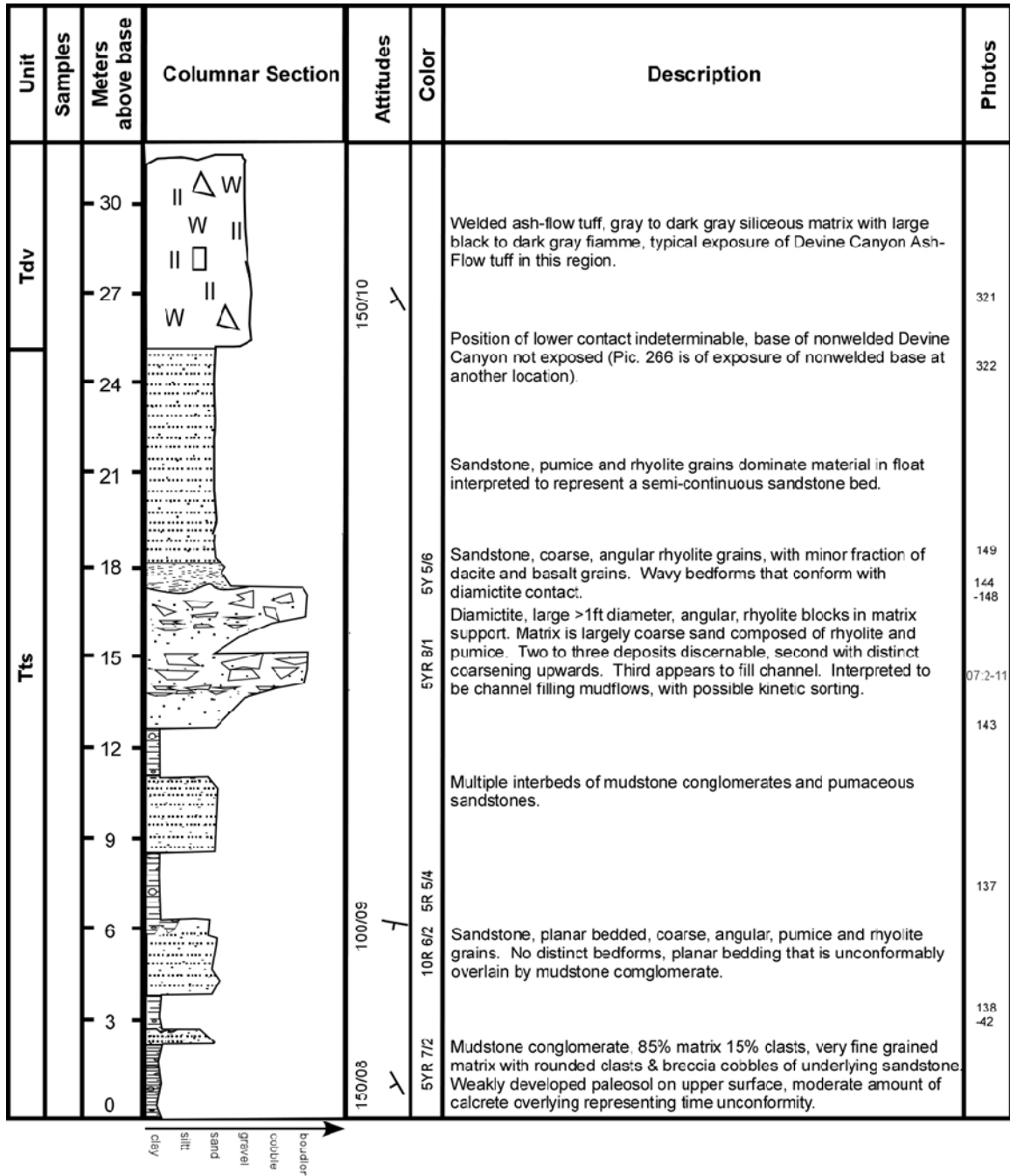
Appendix Figure 2 continued...



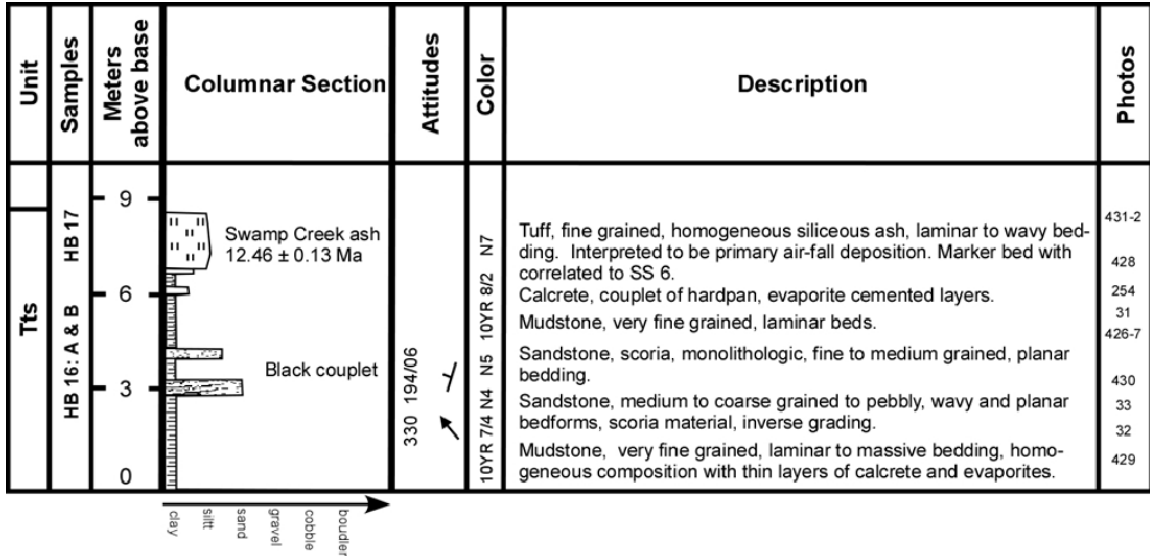
Appendix Figure 2 continued...

Unit	Samples	Meters above base	Columnar Section	Attitudes	Color	Description	Photos
Tdw		156			10YR 4/2 6Y 3/2	Basalt, monolithic autobrecciated base and top.	423-4
		153			10YR 6/6	Basalt, autobreccia base, vesicles, distinguishable separate small flows with toes and margins. Oxidized flowtop with thin autobreccia. Observations suggest a sub aerial flow.	422
		150			10R 6/6	Tuffaceous mudstone; pumice grains, and ash. Angular clasts 1mm-2cm diameter, bedding indistinguishable. Irregular lower contact and baked upper contact with overlying basalt.	420-1
		147			5R 2/2	Breccia, clast support, scoria and basalt dominated, clast size 6cm to 1 meter in diameter, includes spindle bombs.	418-5
		144			N8 5R 6/6	Hydrothermally alter breccia, red to orange staining in matrix and rinds on clasts. Clasts a largely silicic, 60-75% pumice with minor amounts of scoria.	417
		141			5R 2/6	Breccia, 80 % scoria clasts, with minor amounts of pumice and rhyolite. Clasts in weak matrix support bordering on clasts support, matrix dominantly mafic ash and minor pumice.	416
		138				Sandstone, medium to fine grained, subangular grains, weakly developed planar beds.	415
		135			N7-N8	Sandstone, medium to fine grained, subangular to subrounded grains, weakly developed crossbedding.	
		133				Conglomerates, pebbly sandstones, siltstones, silty mudstones, that are interbedded, normally graded, well rounded, majority display tabular bedding, dominated by pumaceous detritus >95%.	
		132					

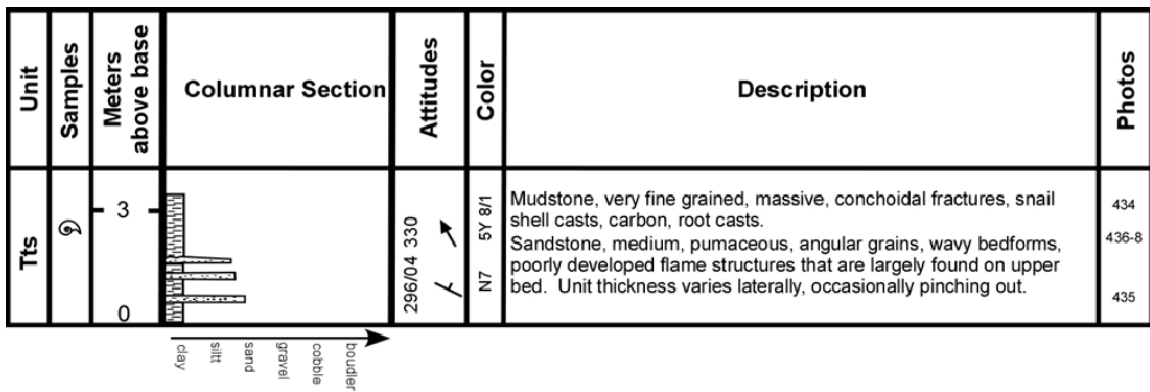
Appendix Figure 2 continued...



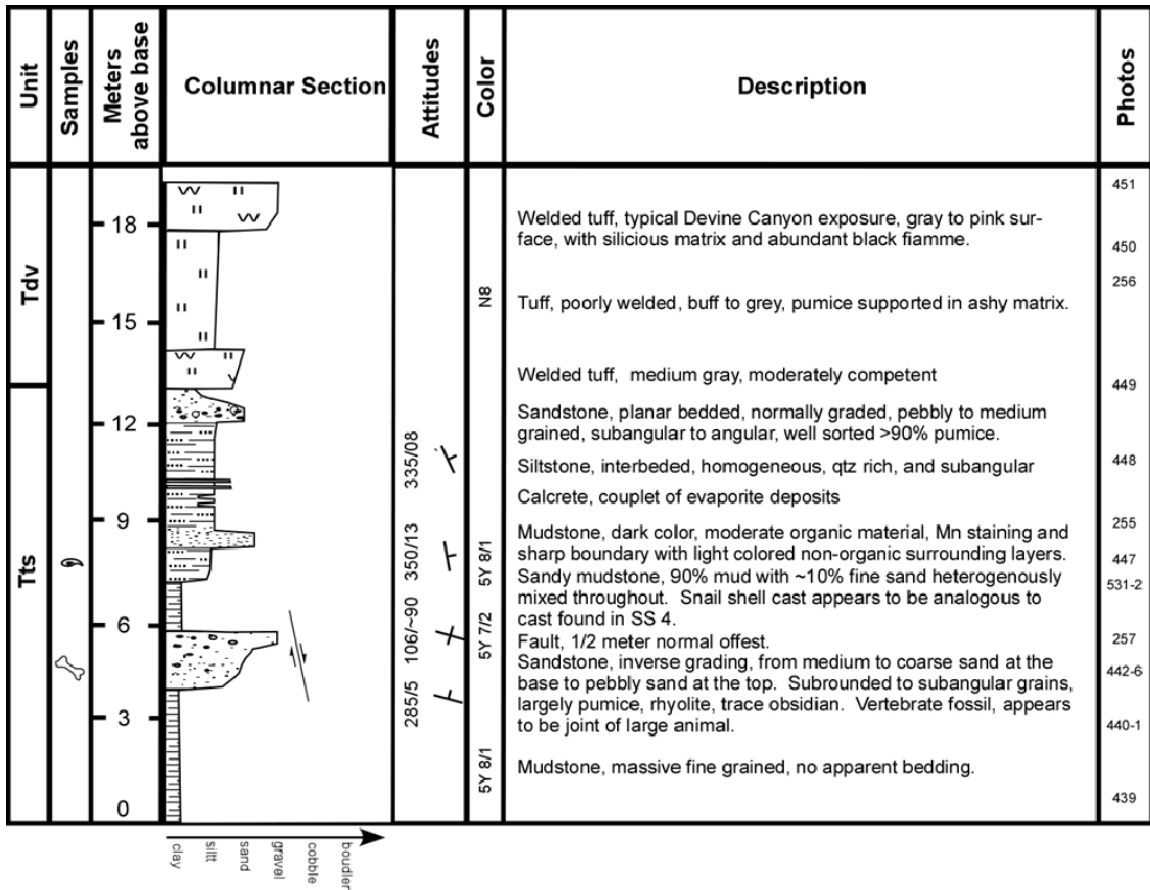
Appendix Figure 3. Stratigraphic Section 2 of the Tts unit. Column represents a high energy depositional environment at the margins of the Crane Basin. Here, depositional processes likely ranged from fluvial and aerial to landslides and mudflows.



Appendix Figure 4. Stratigraphic Section 3 measured near the center of the Eastern Crane Basin that represents a playa-like depositional environment. Lithologies vary from clays to sandstones to evaporates. The black couplet of scoria sandstone found midway through the section and the overlying air-fall ash at the top can be correlated to analogous deposits in Stratigraphic Section 6.



Appendix Figure 5. Stratigraphic Section 4 clearly illustrates the lacustrine and playa-like environment of the Crane Basin. Few depositional events possessed the energy and sediment volume to reach the center of the basin, marked by the anomalous fine grained sandstones within the dominantly clay sediment column.

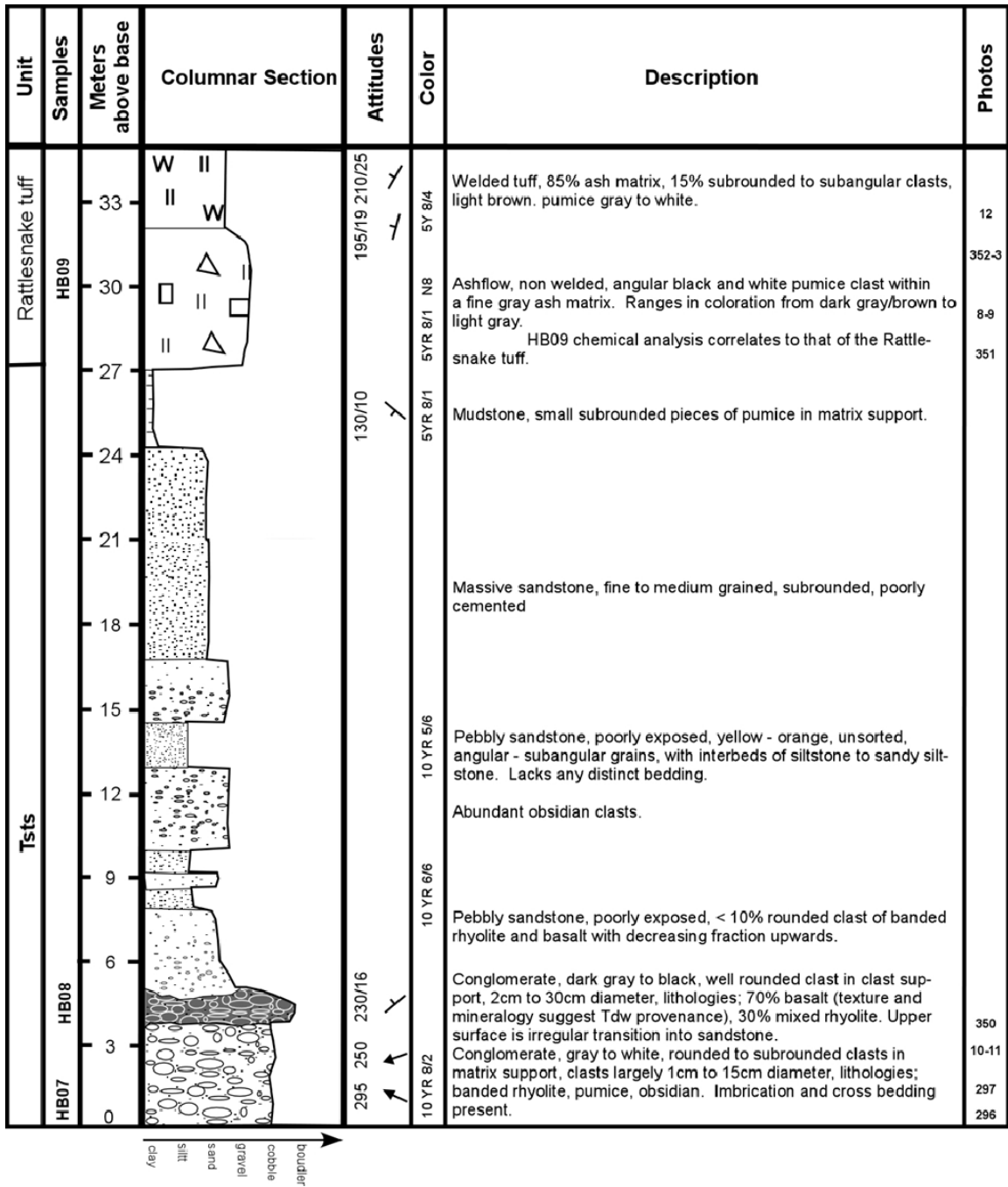


Appendix Figure 6. Stratigraphic Section 5 of Tts in the center of the Crane Basin can be correlated to Stratigraphic Section 2 at the margins via the Devine Canyon tuff. A distinct contrast between the two sections in lithology illustrates the variance in intrabasinal depositional environments.

Unit	Samples	Meters above base	Columnar Section	Attitudes	Color	Description	Photos
Tts	HB14	0-6	<p>clay silt sand gravel cobbles Black couplet Swamp Creek ash 12.46 ± 0.13 Ma</p>	<p>303/82 140/10 315/72 190/05</p>	<p>N2 5R 6/2 N8 10YR 5/4</p>	<p>Cobble and mudstone conglomerate, series of deposits with clasts size increasing upwards. Uppermost unit possesses angular clasts composed of middle unit, 55% clast &amp; 45% matrix. Lowest unit is 95% mudstone matrix with 10% pumice &amp; rhyolite clasts.</p> <p>Fine grained ash, 95% glass shards. Lower bed is massive with weakly developed bedding and waveforms. Upper bed has strongly developed planar beds, decreasing thickness upwards. Contact between beds exhibits soft sediment deformation. Basal contact is normally offset ~1.5 meters.</p> <p>Silty mudstone, fine grained, massive bedding, two interbeds of dark gray sandstone. Cut by fault with 1/3 meter offset.</p>	<p>459-60 293 290-1 461-2 455-6 458 454 288-9 452-3</p>

Appendix Figure 7. Stratigraphic Section 6 represents a small basin isolated from the greater Crane Basin as inferred from paleo-topographic highs of Tba and Trd that would have created drainage divides between the two depocenters. The key observation is the presence of both the black scoria sandstone couplet and the air-fall ash in the stratigraphic column. The black couplet suggests both basins possessed similar provenance that provided the same detritus. Also, neither of these two marker beds have been found west of the Crane Basin, suggesting the existence of a local drainage divide. The author notes that the lack of the ash westward could also be attributed to a combination of source location and prevailing westerly winds.





Appendix Figure 8. Stratigraphic section 7 of an anomalous section of volcaniclastic sediment (Tstt) that underlies the Rattlesnake tuff (See Figure 4). Section reflects a fluvial depositional environment that has been interpreted to be responsible for quickly incising a channel through Tdw and the underlying Tdw and Tsts sediments.

## 40Ar/39Ar Dating

### **Methods**

Six samples were analyzed at the Oregon State University Noble Gas Mass Spectrometry lab in the College of Oceanic and Atmosphere Sciences. Samples included four basalts and two air-fall ashes. Two of the basalts were prepared as plagioclase separates (HB02 & HB10), one as a groundmass (HB13) and one as a whole rock core (HB15). Ash sample HB14 lacked any appreciable potassium rich phases so it was prepared as a glass separate. Ash sample HB17 possessed ample plagioclase and was prepared as such.

Samples were prepared following standard operation procedures prescribed by the laboratory for both plagioclase separates and whole-rock minicores. Following preparation, samples and monitors (Fish Canyon Tuff biotite, FCT-3, with a reference age of 28.02 Ma (Renne, 1994)) were stacked in quartz tubes, then irradiated in the Cd-shielded cadmium-lined, in-core irradiation tube (CLICIT) facility of the Oregon State University TRIGA experimental reactor.

Five samples were analyzed by the laser total fusion method using a MechanteK integrated CO<sub>2</sub> continuous fire laser with infrared pyrometer gas extraction system. Each system is connected to an ultra-clean, low volume gas cleanup line with Zr-AL and Zr-V-Fe getters. For gas extraction using the resistance furnace the whole rock sample was loaded into a sample manifold and then into a Ta/Nb-crucible with a Mo-liner. Temperatures are precisely controlled for the incremental heating steps. For gas extraction using the laser, mineral separates were loaded into a Cu-planchette that is placed in a high vacuum chamber fitted with a ZnS window that is transparent to the CO<sub>2</sub> laser wavelength. Temperatures of incremental heating steps are monitored with an infrared pyrometer. Analyses were made on a Mass Analyser Products model 215-50 rare gas spectrometer with an all-metal extraction system.

## **Results**

All six analyses are fully displayed in the appendix. Four of the six were successful displays of a statistically valid weighted plateau; the other two were statistically irrelevant. Starting with the air-fall ashes from within Tsts unit, sample HB14's weighted plateau age is  $12.48 \pm 0.13$  Ma and sample HB17's is  $12.45 \pm 0.13$  Ma. The similar stratigraphic location of both samples, overlying a basaltic pebbly sandstone suggest that both samples represent a geographically correlative air-fall ash. This observation is further supported by the extremely similar ages calculated on both samples. Exposures of gray air fall ashes in separate locals along Hwy 20 northwest of these sample's local should be noted at this time, suggesting this previously undescribed ash could be a regional marker bed here named, the Swamp Creek ash.

Three basalt samples dated were chosen to constrain the ages of the two Tdw flows, one of which filled in the Eastern Crane Basin and the other filled in the Western Crane Basin. One sample was taken for the eastern Tdw and two for the western Tdw. Two were taken from the western basalt because a dike was exposed whose field relationships suggest it fed the surface flow of which a sample was also taken. Unfortunately the samples from the western flow (HB02 and HB10) provided poor material for dating and erroneous dates (See Table 1 in the appendix). The eastern flow (sample HB15) provided a date of  $7.25 \pm 0.09$  Ma. Due to the similar characteristics of both the eastern and western Tdw flows and their analogous lithostratigraphic locations it is safe to assume the western flow erupted relatively contemporaneously with the eastern flow. A previous date by Walker (1979) on the western flow of  $\sim 7$  Ma supports this assumption.

The final sample (HB13) was of the Voltage basalt (Qb) that flowed down the modern stream gradient of the south fork of the Malheur River. Its weighted plateau age is  $1.93 \pm 0.29$  Ma.

Table 1. Summary of $^{40}\text{Ar}$ - $^{39}\text{Ar}$ re-sults.										
*Sample No.	Latitude	Longitude	Type	Material dated	analysis	Steps	% $^{39}\text{Ar}$	K/Ca	age (Ma)	2 $\sigma$
HB02	43.3548	-118.5517	Basalt	plagioclase	plateau	8	100	0.008	4.57	2.4
HB10	43.3681	-118.4817	Basalt	plagioclase	plateau	10	29.69	0.01	11.88	4.87
HB13	43.4060	-118.2850	Basalt	groundmass	plateau	7	98.52	0.019	1.93	0.29
HB14	43.3906	-118.2822	Air-fall ash	glass	plateau	9	92.56	1.321	12.48	0.03
HB15	43.3845	-118.1708	Basalt	wholerock	plateau	9	94.47	0.127	7.25	0.09
HB17	43.3611	-118.1767	Air-fall ash	plagioclase	plateau	11	93.79	0.242	12.45	0.03

Appendix Table 1. Data for all Crane Basin study area samples that were analyzed for  $^{40}\text{Ar}/^{39}\text{Ar}$  dating.

## XRF and ICP-MS Geochemistry

### Methods

Eight samples were chosen to be analyzed at the Washington State University GeoAnalytical Laboratory (Tables 2 & 3). Samples included the basalts being dated, as well as two pumice separates from unidentified ignimbrites. The two ignimbrite samples were chosen because their stratigraphic location within the Tsts unit made them candidates for being isolated deposits of the Devine Canyon (DC), Prater Creek (PC) or Rattlesnake (RS) ash-flow tuffs. Depending upon the correct identification of the two samples different interpretations for the depositional history of the Western Crane Basin are plausible. By comparing the geochemistry of the samples (HB01 and HB09) to the known geochemistry of these ignimbrites a confident correlation will identify them. Representative samples of DC, PC, and RS were chosen that also had known  $^{40}\text{Ar}/^{39}\text{Ar}$  dates identifying them as such. Streck found 5 distinct variations (Groups A – E) of the RS pumices (Streck, 1995; Streck, 1999), end members A and E were used in this study. The intention being, constraining a possible RS sample to within the variation of RS geochemistry's between end member samples of Streck. Comparison of chemistries focused strictly upon the less mobile High Field Strength (HFS) elements (Y, Hf, Zr, Ti, Nb, Ta) (Rollinson, 1993). Limiting our analysis to these elements due to the evidence of alteration to both samples seen in the low totals of the unnormalized major elements (HB01 86.33 weight %, HB09 87.04 weight %, see Table 3).

All steps of preparation and analyses followed the guidelines set by WSU laboratory (Johnson D. M., 1999). Samples were cleaned and crushed to 1cm diameter chips. For XRF analysis chips were ground with tungsten carbide surfaces, and then properly weighed and mixed with pure dilithium tetraborate. Mixed samples were fused at 1,000° C, cooled, re-ground and fused again. Following the second fusion the beads were labeled with an engraver,

the lower flat surface is ground on 600 silicon carbide grit and a finished surface is done on a glass plate. Final cleaning was done via an ultrasonic bath and alcohol rinse.

All steps of preparation and analyses followed the guidelines set by WSU (Knaack, 1994). For ICP-MS analysis the same preparation was done with the exception of using an iron bowl to crush chips to a powder and there was no second fusion. Following the first fusion the bead is crushed and then standard operating procedures were followed for acidic dissolution for a final preparation to ensure complete dissolution of refractory phases.

In all cases data has been normalized to 100 % volatile free, followed by normalization to Chondrite C1 (McDonough, 1995) in analyses.

## **Results**

The results of the study were surprising and altogether enlightening. Initially HB01 was hypothesized to be either the Prater Creek or Rattlesnake tuffs due to its location. Geochemical comparison of HB01 to all three ignimbrites indicates it most closely resembles the composition of the Devine Canyon tuff. Values of  $\gamma$ , Zr, Nb, Hf, Ta, and U are near matches for HB01, MTF-07 and JJ 93-1. HB09 was hypothesized to Rattlesnake tuff largely based upon its character in outcrop and hand sample. Pumices varied from white to gray to black, a characteristic solely seen within the Rattlesnake tuff and described by Streck (1995). HB09 is anomalously high in the compatible elements, likely a result of alteration via weathering but it also has anomalously low values in many of the incompatible elements. Though, when it does match up with values of other samples it is most often RT165E or RT134A, such as Nb, Ta, and U. HB09 and RT344 are the only samples with high Ba. Combining both the field and geochemical evidence a confident assertion can be made that HB09 is the Rattlesnake tuff.

**Table 2. Summary of ICPMS analysis**

*Sample No.	Rock Type	State	County	Latitude	Longitude	La ppm	Ce ppm	Pr ppm	
1 HB01	pumice	OR	Hamey	43.3548	118.5498	79.31	170.05	22.26	
2 HB02	Basalt	OR	Hamey	43.3550	118.5508	9.78	20.33	3.19	
3 HB03	Basalt	OR	Hamey	43.3634	118.5313	16.43	36.59	5.07	
4 HB09	pumice	OR	Hamey	43.3679	118.4818	20.49	39.71	5.33	
5 HB10	Basalt	OR	Hamey	43.3701	118.4851	17.04	37.76	5.21	
6 HB13	Basalt	OR	Hamey	43.4060	118.2855	4.70	10.72	1.65	
7 HB15	Basalt	OR	Hamey	43.3848	118.1672	16.98	34.43	4.73	
8 HB19	Basalt	OR	Hamey	43.4126	118.3183	13.61	25.28	3.36	
1R SAB HB01 @fb						79.74	170.01	22.23	
Pr ppm	Nd ppm	Sm ppm	Eu ppm	Gd ppm	Tb ppm	Dy ppm	Ho ppm	Er ppm	
1	22.26	89.46	23.17	0.66	24.01	4.50	29.28	6.26	17.56
2	3.19	15.22	4.26	1.60	4.98	0.87	5.44	1.15	3.16
3	5.07	22.74	5.83	2.07	6.20	1.05	6.51	1.34	3.60
4	5.33	21.08	5.03	0.90	5.39	1.01	6.70	1.48	4.24
5	5.21	23.24	5.89	2.15	6.33	1.06	6.63	1.36	3.61
6	1.65	8.04	2.46	0.97	3.05	0.55	3.68	0.77	2.13
7	4.73	20.38	5.09	1.70	5.40	0.92	5.82	1.21	3.23
8	3.36	14.29	3.66	1.29	4.28	0.74	4.66	0.99	2.67
1R	22.23	89.38	23.39	0.66	24.36	4.55	29.36	6.22	17.62
Tm ppm	Yb ppm	Lu ppm	Ba ppm	Th ppm	Nb ppm	Y ppm	Hf ppm	Ta ppm	
1	2.63	16.65	2.62	17	15.75	89.57	161.72	28.55	5.65
2	0.45	2.71	0.44	304	0.49	5.20	29.82	2.32	0.32
3	0.51	3.18	0.50	453	0.97	11.43	32.91	3.36	0.70
4	0.68	4.54	0.74	620	10.01	22.48	36.66	17.17	2.17
5	0.51	3.17	0.50	476	1.06	11.73	33.21	3.38	0.72
6	0.31	1.94	0.31	130	0.35	2.61	19.09	1.58	0.16
7	0.47	2.94	0.47	842	1.34	8.38	30.23	3.88	0.50
8	0.39	2.44	0.38	592	1.59	5.78	25.79	3.27	0.37
1R	2.64	16.84	2.63	18	15.83	89.70	162.28	28.72	5.68
U ppm	Pb ppm	Rb ppm	Cs ppm	Sr ppm	Sc ppm	Zr ppm			
1	6.27	33.59	153.2	4.73	47	1.1	1329		
2	0.17	1.50	4.3	0.07	305	37.5	89		
3	0.34	3.07	12.0	3.15	280	31.4	133		
4	2.17	7.31	34.7	1.39	67	11.4	580		
5	0.37	3.37	10.3	0.11	267	32.2	136		
6	0.12	0.91	3.0	0.05	196	31.6	60		
7	0.40	3.92	20.9	0.24	292	28.0	158		
8	0.44	3.87	25.3	0.31	223	25.9	130		
1R	6.27	33.58	152.5	4.69	48	1.1	1319		

\* Sample numbers correspond to map illustrated on Figure#.

Appendix Table 2. Trace element geochemical data analyzed at the Washington State University laboratory.



Table 3. Summary of XRF analyses.

	*HB01	HB02	HB03	*HB09	HB10	HB13	HB15	HB19	HB01R
Date	18-Feb-09	18-Feb-09	18-Feb-09	19-Feb-09	19-Feb-09	19-Feb-09	19-Feb-09	19-Feb-09	21-Feb-09
<b>Unnormalized Major Elements (Weight %):</b>									
SiO <sub>2</sub>	64.86	48.41	47.31	54.79	47.26	48.50	51.63	53.43	64.85
TiO <sub>2</sub>	0.159	1.376	1.989	0.409	2.004	0.906	1.365	1.118	0.153
Al <sub>2</sub> O <sub>3</sub>	9.30	17.02	16.34	23.01	16.12	16.98	16.09	16.63	9.25
FeO*	2.51	10.40	11.01	4.58	11.12	9.62	9.03	7.97	2.51
MnO	0.051	0.187	0.187	0.030	0.180	0.174	0.167	0.145	0.051
MgO	0.37	7.67	7.29	0.80	7.27	9.32	6.41	6.50	0.35
CaO	0.71	10.85	9.43	0.86	9.47	11.14	9.03	8.56	0.69
Na <sub>2</sub> O	2.69	2.74	2.74	0.99	2.77	2.59	2.85	2.73	2.70
K <sub>2</sub> O	5.65	0.41	0.83	1.55	0.76	0.25	1.35	1.62	5.65
P <sub>2</sub> O <sub>5</sub>	0.023	0.315	0.466	0.017	0.478	0.111	0.340	0.141	0.022
Sum	86.33	99.38	97.59	87.04	97.44	99.58	98.25	98.85	86.24
SO <sub>3</sub> >=	0.08	0.00	0.01	0.00	0.03	0.01	0.06	0.00	0.11
Cl >=	0.16	0.00	0.00	0.00	0.00	0.00	0.00	0.00	0.15
<b>Normalized Major Elements (Weight %):</b>									
SiO <sub>2</sub>	75.14	48.71	48.48	62.95	48.50	48.71	52.54	54.05	75.20
TiO <sub>2</sub>	0.184	1.385	2.038	0.469	2.056	0.909	1.390	1.131	0.178
Al <sub>2</sub> O <sub>3</sub>	10.77	17.13	16.75	26.43	16.54	17.05	16.38	16.83	10.73
FeO*	2.91	10.46	11.28	5.27	11.41	9.66	9.19	8.07	2.91
MnO	0.059	0.188	0.192	0.034	0.185	0.174	0.170	0.147	0.059
MgO	0.42	7.71	7.47	0.92	7.46	9.35	6.52	6.58	0.40
CaO	0.82	10.92	9.66	0.99	9.72	11.18	9.19	8.66	0.80
Na <sub>2</sub> O	3.12	2.76	2.81	1.14	2.85	2.60	2.90	2.76	3.13
K <sub>2</sub> O	6.55	0.41	0.85	1.78	0.78	0.25	1.37	1.64	6.56
P <sub>2</sub> O <sub>5</sub>	0.027	0.317	0.478	0.019	0.490	0.112	0.346	0.143	0.026
Total	100.00	100.00	100.00	100.00	100.00	100.00	100.00	100.00	100.00
<b>Unnormalized Trace Elements (ppm):</b>									
Ni	0	127	100	1	103	174	100	96	1
Cr	2	205	195	15	176	361	141	78	1
Sc	1	37	35	12	34	33	29	29	1
V	3	277	276	52	272	238	205	186	1
Ba	15	311	465	630	487	129	864	606	15
Rb	143	4	12	36	10	3	21	26	143
Sr	40	297	281	68	267	199	294	223	41
Zr	1163	91	136	594	140	63	162	132	1165
Y	152	29	34	37	34	20	30	25	153
Nb	83.0	4.6	11.2	23.9	11.7	2.8	7.7	5.1	83.6
Ga	26	16	17	38	17	15	16	16	26
Cu	9	75	70	8	68	69	65	53	10
Zn	254	85	98	171	103	71	81	68	252
Pb	33	2	3	7	3	1	3	3	32
La	73	11	17	20	17	4	15	14	75
Ce	163	17	36	40	36	9	36	24	159
Th	18	2	2	12	2	1	2	2	19
Nd	83	15	23	21	23	7	23	16	82
U	6	1	1	3	0	0	3	1	6
Cs	5	0	1	1	1	0	0	1	3

Appendix Table 3. Major element geochemical data analyzed at the Washington State University laboratory.

sum tr.	2272	1605	1813	1788	1804	1396	2097	1603	2267
in %	0.23	0.16	0.18	0.18	0.18	0.14	0.21	0.16	0.23
sum m+tr	86.55	99.54	97.77	87.22	97.62	99.72	98.46	99.01	86.46
M+Toxides	86.62	99.59	97.82	87.26	97.67	99.77	98.51	99.05	86.24
Major elements are normalized on a volatile-free basis, with total Fe expressed as FeO.									
	*HB01	HB02	HB03	*HB09	HB10	HB13	HB15	HB19	HB01R
NiO	0.0	161.6	127.2	0.9	131.2	221.0	127.1	122.3	0.7
Cr2O3	3.4	299.5	284.3	21.8	257.4	527.0	206.5	113.7	1.9
Sc2O3	1.5	56.6	52.9	19.0	51.7	50.3	44.8	44.0	0.9
V2O3	4.4	407.4	406.0	76.4	400.4	349.5	301.1	273.0	1.3
BaO	17.1	347.1	519.1	703.8	543.4	144.4	964.4	676.7	16.5
Rb2O	155.9	4.8	12.9	39.5	11.0	2.7	23.4	28.0	156.5
SrO	47.8	350.8	332.1	79.9	315.3	234.7	347.3	263.5	48.5
ZrO2	1570.3	122.8	184.0	801.7	189.1	85.1	218.3	178.3	1573.5
Y2O3	192.7	36.2	42.9	47.2	42.7	25.1	38.1	32.3	193.8
Nb2O5	118.7	6.6	16.0	34.2	16.7	4.0	11.0	7.3	119.6
Ga2O3	34.4	21.5	22.9	50.9	23.0	19.8	21.8	21.9	34.5
CuO	11.4	93.8	88.1	9.5	84.7	85.9	80.7	66.1	12.4
ZnO	317.8	106.5	122.6	214.4	129.1	88.6	101.8	84.7	315.0
PbO	35.4	1.6	3.6	7.2	3.6	0.6	3.0	3.6	34.9
La2O3	86.0	12.4	20.3	23.1	19.9	4.2	17.5	16.7	88.4
CeO2	200.6	21.0	44.3	49.0	44.0	10.7	44.3	29.6	195.3
ThO2	20.1	2.4	2.1	13.4	2.2	1.1	2.1	1.8	20.7
Nd2O3	96.2	17.5	27.2	24.4	26.8	8.5	26.8	18.7	95.8
U2O3	6.6	0.8	1.2	2.9	0.0	0.0	3.2	1.4	6.2
Bi2O5	0.0	0.0	0.0	0.0	0.0	0.0	0.0	0.0	0.0
Cs2O	5.5	0.0	1.3	1.0	0.7	0.0	0.0	0.5	3.4
As2O5	0.0	0.0	0.0	0.0	0.0	0.0	0.0	0.0	0.0
W2O3	0.0	0.0	0.0	0.0	0.0	0.0	0.0	0.0	0.0
sum tr.	2926	2071	2311	2220	2293	1863	2583	1984	2920
in %	0.29	0.21	0.23	0.22	0.23	0.19	0.26	0.20	
* Notes samples that possessed anominously low totals from first analyses. Data shown are from second analyses with loss of ignition.									
"R" denotes a duplicate bead made from the same rock powder.									

Appendix Table 3 continued...

Table 4. Summary of geochemistry used in Figure 6. (ppm)

	HB01	HB09	*RT165E	*RT34A	**JJ 93-124	***MTF 07-10	****PC-134.1	****PC-146
Na	11576.65	5317.24	14441.80	13272.17	18064.39	13774.20	13713.08	13849.90
Mg	2549.93	4322.29	0.00	725.28	0.00	472.51	6.06	200.28
Al	28499.01	123566.77	31968.68	32941.31	26860.01	28725.40	31742.21	32279.07
Si	351226.61	294239.28	363053.12	352874.79	352453.96	357777.92	354591.47	354904.17
P	57.96	91.03	43.68	43.74	21.82	28.43	24.11	24.16
K	27183.60	8329.28	21021.06	23171.87	19134.96	22794.56	23876.51	22975.65
Sc	1.10	11.37	4.05	4.29	1.38	1.09	1.67	1.59
Ti	1102.40	2193.99	660.04	1021.48	1378.88	1187.22	903.41	874.87
V	3.00	51.90	2.50	7.70	n.a.	2.00	1.50	1.10
Cr	2.30	14.90	1.60	4.20	3.00	2.10	1.80	3.95
Mn	458.88	159.40	620.11	698.59	542.12	435.32	365.67	397.51
Fe	22630.12	24616.03	6014.96	15618.56	34590.53	21741.26	17345.14	16806.24
Ni	0.00	0.71	14.00	8.40	21.00	n.a.	9.90	10.90
Cu	9.10	7.60	1.20	3.10	5.00	6.00	10.30	5.20
Zn	253.70	171.20	88.00	117.00	262.00	233.90	105.80	108.50
Ga	25.60	37.90	17.80	19.00	30.00	27.30	20.20	20.50
Se	5855.59	4610.26	n.a.	n.a.	n.a.	n.a.	n.a.	n.a.
Rb	142.60	36.10	123.00	63.00	212.00	134.49	100.40	99.60
Sr	47.32	66.67	3.40	23.90	8.00	6.11	14.30	10.90
Y	151.70	37.20	101.00	76.00	156.00	144.21	79.90	83.90
Zr	1329.41	580.31	175.00	457.00	813.00	1157.37	542.10	555.00
Nb	83.00	23.90	40.30	25.60	42.00	80.46	48.50	49.10
Cs	4.73	1.39	4.54	2.28	5.29	4.42	2.56	2.60
Ba	15.30	630.40	25.00	1947.00	45.00	36.49	91.00	100.00
La	79.31	20.49	21.70	51.10	89.40	90.00	59.00	66.60
Ce	170.05	39.71	54.00	112.00	214.00	187.96	129.00	132.00
Pr	22.26	5.33	n.a.	n.a.	n.a.	n.a.	n.a.	n.a.
Nd	89.46	21.08	30.00	52.00	102.00	93.36	53.00	58.00
Sm	23.17	5.03	9.58	12.85	25.00	22.45	10.69	12.66
Eu	0.66	0.90	0.65	2.56	2.23	0.72	0.29	0.35
Gd	24.01	5.39	n.a.	n.a.	n.a.	n.a.	n.a.	n.a.
Tb	4.50	1.01	2.30	2.17	4.41	4.13	1.86	2.13
Dy	29.28	6.70	n.a.	n.a.	n.a.	n.a.	n.a.	n.a.
Ho	6.26	1.48	n.a.	n.a.	n.a.	n.a.	n.a.	n.a.
Er	17.56	4.24	n.a.	n.a.	n.a.	n.a.	n.a.	n.a.
Tm	2.63	0.68	n.a.	n.a.	n.a.	n.a.	n.a.	n.a.
Yb	16.65	4.54	10.55	7.68	15.80	15.16	8.27	8.77
Lu	2.62	0.74	1.62	1.16	2.29	2.39	1.23	1.35
Hf	28.55	17.17	7.24	11.17	25.90	25.63	13.48	13.40
Ta	5.65	2.17	2.28	1.33	2.72	4.97	2.64	2.76
Pb	33.59	7.31	18.90	15.40	21.00	30.97	9.60	17.90
Th	18.20	12.10	9.87	5.63	23.30	14.02	8.90	9.10
U	6.27	2.17	4.48	2.30	9.85	5.71	4.39	3.83

\* (Streck, 1999), \*\* (Johnson 1995), \*\*\* (Ford, In Preparation), \*\*\*\* (Jordan, 2002)

Appendix Table 4. Geochemical data used in Crane Basin tuff comparison.

Incremental Heating	36Ar(a)	37Ar(ca)	38Ar(c)	39Ar(k)	40Ar(i)	Age ± 2σ (Ma)	40Ar(i) (%)	39Ar(k) (%)	K/Ca ± 2σ
09C2173	0.008027	0.062643	0.000320	0.032496	0.024534	2.16 ± 5.08	1.02	12.51	0.223 ± 0.013
09C2174	0.004244	0.317354	0.000377	0.060724	0.036648	1.72 ± 0.76	2.84	23.37	0.082 ± 0.005
09C2175	0.002078	0.464221	0.000228	0.052514	0.033706	1.83 ± 0.45	5.20	20.21	0.049 ± 0.003
09C2176	0.001276	0.476474	0.000090	0.045080	0.037137	2.35 ± 0.35	8.96	17.35	0.041 ± 0.002
09C2178	0.000954	0.361477	0.000024	0.031631	0.018040	1.63 ± 0.35	6.02	12.17	0.038 ± 0.002
09C2179	0.000843	0.355941	0.000022	0.019678	0.007305	1.06 ± 1.48	2.85	7.57	0.024 ± 0.001
09C2180	0.000763	0.520291	0.000000	0.013897	0.013737	2.82 ± 1.52	5.75	5.35	0.011 ± 0.001
09C2182	0.000335	0.199057	0.000000	0.003841	0.000000	0.00 ± 0.00	0.00	1.48	0.008 ± 0.000
Σ	0.018520	2.757458	0.001061	0.259860	0.171106				

Information on Analysis	Results	40(i)/39(k) ± 2σ	Age ± 2σ (Ma)	MSWD	39Ar(k) (%)	K/Ca ± 2σ
HLP JBM HB13 glass 1D13-09	<b>Weighted Plateau</b>	0.6761 ± 0.1013 ± 14.98%	1.93 ± 0.29 ± 14.99%	1.99	98.52	0.019 ± 0.013
HLP			External Error ± 0.29	2.45	7	Statistical T Ratio
JBM			Analytical Error ± 0.29	1.4107		Error Magnification
Project = HLP	<b>Total Fusion Age</b>	0.6585 ± 0.2394 ± 36.36%	1.88 ± 0.68 ± 36.35%		8	0.041 ± 0.001
Irradiation = OSU1D09			External Error ± 0.68			
J = 0.0015848 ± 0.0000065			Analytical Error ± 0.68			
FCT-3 = 28.030 ± 0.003 Ma						

Appendix Table 5. Complete data from Noble Gas Spectrometry Laboratory analysis on sample HB13 (Voltage Basalt)

Incremental Heating	36Ar(a)	37Ar(ca)	38Ar(c)	39Ar(k)	40Ar(r)	Age $\pm 2\sigma$ (Ma)	40Ar(r) (%)	39Ar(k) (%)	K/Ca $\pm 2\sigma$
09C2159	500 °C	0.005060	0.082843	0.000541	0.162957	12.77 $\pm 0.48$	32.52	7.10	0.846 $\pm 0.049$
09C2160	600 °C	0.003051	0.052138	0.001264	0.323406	12.48 $\pm 0.19$	60.78	14.09	2.667 $\pm 0.152$
09C2161	700 °C	0.002250	0.040704	0.002234	0.529427	12.41 $\pm 0.08$	77.36	23.07	5.593 $\pm 0.326$
09C2162	775 °C	0.001757	0.036665	0.002491	0.577450	12.47 $\pm 0.05$	82.74	25.16	6.772 $\pm 0.385$
09C2164	850 °C	0.001139	0.021157	0.001481	0.344667	12.62 $\pm 0.17$	81.72	15.02	7.005 $\pm 0.400$
09C2165	925 °C	0.000870	0.011488	0.000795	0.186464	12.81 $\pm 0.18$	76.27	8.12	6.979 $\pm 0.427$
09C2166	1025 °C	0.000444	0.006221	0.000442	0.098282	14.05 $\pm 0.10$	78.46	4.28	6.793 $\pm 0.425$
09C2169	1125 °C	0.000190	0.002200	0.000149	0.036903	14.86 $\pm 0.35$	77.15	1.61	7.213 $\pm 0.870$
09C2170	1225 °C	0.000177	0.001516	0.000072	0.018485	16.02 $\pm 0.65$	66.19	0.81	5.243 $\pm 0.570$
09C2171	1400 °C	0.000361	0.001672	0.000086	0.017069	16.16 $\pm 0.84$	47.27	0.74	4.389 $\pm 0.401$
$\Sigma$		0.015300	0.256605	0.009556	2.295109	10.083640			

Information on Analysis	Results	40(t)/39(k) $\pm 2\sigma$	Age $\pm 2\sigma$ (Ma)	QMS (%)	39Ar(k) (% n)	K/Ca $\pm 2\sigma$
-------------------------	---------	---------------------------	------------------------	---------	---------------	--------------------

HLP JBM HB14 1D12-09  
glass  
HLP  
JBM

**Error Plateau** 4.3206  $\pm 0.0284$   $\pm 0.66\%$  12.48  $\pm 0.13$   $\pm 1.02\%$  4.16 92.56 1.321  $\pm 1.222$

External Error  $\pm 0.24$  2.57 Statistical T Ratio  
Analytical Error  $\pm 0.08$  2.0403 Error Magnification

Project = HLP  
Irradiation = OSU1D09  
J = 0.0016067  $\pm 0.0000063$   
FCT-3 = 28.030  $\pm 0.003$  Ma

**Total Fusion Age** 4.3935  $\pm 0.0202$   $\pm 0.46\%$  12.69  $\pm 0.11$   $\pm 0.90\%$  10 3.846  $\pm 0.099$

External Error  $\pm 0.23$   
Analytical Error  $\pm 0.06$

Appendix Table 6. Complete data from Noble Gas Spectrometry Laboratory analysis on sample HB14 (Swamp Creek Ash)

Incremental Heating	36Ar(a)	37Ar(ca)	38Ar(c)	39Ar(k)	40Ar(f)	Age $\pm 2\sigma$ (Ma)	40Ar(f) 39Ar(k) (%) (%)	K/Ca $\pm 2\sigma$
09C1520	500 °C	0.016745	0.227443	0.009104	0.758236	2.045360	7.20 $\pm 0.27$	29.24 25.71 1.434 $\pm 0.049$
09C1521	600 °C	0.005496	0.212599	0.005035	0.447751	1.204906	7.18 $\pm 0.09$	42.59 15.19 0.906 $\pm 0.031$
09C1522	700 °C	0.003948	0.563012	0.004188	0.502023	1.371603	7.29 $\pm 0.05$	54.03 17.03 0.383 $\pm 0.013$
09C1523	800 °C	0.001382	0.948940	0.001198	0.481035	1.309301	7.27 $\pm 0.07$	76.20 16.31 0.218 $\pm 0.008$
09C1524	875 °C	0.000897	1.307432	0.000718	0.442325	1.192491	7.20 $\pm 0.09$	81.79 15.00 0.145 $\pm 0.005$
09C1525	950 °C	0.000535	0.790617	0.000740	0.154297	0.416720	7.21 $\pm 0.08$	72.47 5.23 0.084 $\pm 0.003$
09C1526	1050 °C	0.000365	0.316878	0.001004	0.048031	0.100363	5.58 $\pm 0.26$	48.16 1.63 0.065 $\pm 0.002$
09C1527	1150 °C	0.001175	2.039075	0.001652	0.077553	0.165707	5.71 $\pm 0.32$	32.30 2.63 0.016 $\pm 0.001$
09C1528	1250 °C	0.001189	1.743834	0.000109	0.031288	0.082499	7.04 $\pm 0.81$	19.02 1.06 0.008 $\pm 0.000$
09C1529	1400 °C	0.000345	0.131844	0.000015	0.006098	0.014111	6.18 $\pm 2.46$	12.15 0.21 0.020 $\pm 0.001$
$\Sigma$		0.032078	8.281574	0.023762	2.948637	7.903059		

Information on Analysis	Results	40(t)/39(k) $\pm 2\sigma$	Age $\pm 2\sigma$ (Ma)	$\frac{D}{M}$ $\frac{39Ar(k)}{39Ar(k)}$ (%) (n)	K/Ca $\pm 2\sigma$
JBM HB15 whole rock HLP 1A30-Wholerock	<b>Weighted Plateau</b>	2.7159 $\pm 0.0149$ $\pm 0.55\%$	7.25 $\pm 0.09$ $\pm 1.28\%$	1.58 94.47 6	0.127 $\pm 0.095$
HLP			External Error $\pm 0.15$ Analytical Error $\pm 0.04$	2.57 Statistical T Ratio 1.2572 Error Magnification	
JBM					
Project = HLP Irradiation = OSU1A09 J = 0.0014828 $\pm$ 0.0000086 FCT-3 = 28.030 $\pm$ 0.003 Ma	<b>Total Fusion Age</b>	2.6802 $\pm 0.0277$ $\pm 1.03\%$	7.16 $\pm 0.11$ $\pm 1.55\%$	10	0.153 $\pm 0.002$
			External Error $\pm 0.16$ Analytical Error $\pm 0.07$		

Appendix Table 7. Complete data from Noble Gas Spectrometry Laboratory analysis on sample HB15 (Drinkwater Basalt)

Incremental Heating	36Ar(a)	37Ar(ca)	38Ar(cl)	39Ar(k)	40Ar(r)	Age $\pm 2\sigma$ (Ma)	40Ar(r) 39Ar(k) (%) (%)	K/Ca $\pm 2\sigma$
09C2018	500 °C	0.000552	0.010041	0.000201	0.044232	0.192726	12.24 $\pm 0.49$	54.16 4.83 1.894 $\pm 0.126$
09C2019	600 °C	0.000502	0.061656	0.000447	0.124411	0.548006	12.37 $\pm 0.11$	78.68 13.59 0.868 $\pm 0.046$
09C2020	700 °C	0.000429	0.132689	0.000505	0.161579	0.713475	12.40 $\pm 0.11$	84.89 17.65 0.524 $\pm 0.028$
09C2021	775 °C	0.000432	0.183613	0.000362	0.154510	0.687523	12.50 $\pm 0.13$	84.33 16.88 0.362 $\pm 0.019$
09C2022	850 °C	0.000205	0.155834	0.000175	0.099464	0.442620	12.50 $\pm 0.13$	87.92 10.86 0.274 $\pm 0.015$
09C2024	925 °C	0.000186	0.150229	0.000149	0.082964	0.375437	12.71 $\pm 0.21$	87.24 9.06 0.237 $\pm 0.013$
09C2025	1000 °C	0.000144	0.156687	0.000079	0.075607	0.339292	12.60 $\pm 0.20$	88.87 8.26 0.207 $\pm 0.011$
09C2026	1075 °C	0.000203	0.120107	0.000063	0.054328	0.238719	12.34 $\pm 0.23$	79.90 5.93 0.196 $\pm 0.010$
09C2028	1175 °C	0.000144	0.146305	0.000011	0.061620	0.270953	12.35 $\pm 0.30$	86.39 6.73 0.181 $\pm 0.011$
09C2029	1275 °C	0.000241	0.091788	0.000000	0.037260	0.144783	10.92 $\pm 0.39$	66.98 4.07 0.175 $\pm 0.009$
09C2031	1400 °C	0.000304	0.048586	0.000008	0.019572	0.079479	11.41 $\pm 0.65$	46.92 2.14 0.173 $\pm 0.009$
$\Sigma$		0.003342	1.257534	0.002001	0.915546	4.033012		

Information on Analysis	Results	40(r)/39(k) $\pm 2\sigma$	Age $\pm 2\sigma$ (Ma)	D MSWD	39Ar(k) (% n)	K/Ca $\pm 2\sigma$
JBM HB17 plagioclase Harvey Basin JBM	<b>Weighted Plateau</b>	4.4335 $\pm 0.0251$ $\pm 0.57\%$	12.45 $\pm 0.13$ $\pm 1.06\%$	1.80	93.79 9	0.242 $\pm 0.083$
	<b>Total Fusion Age</b>	4.4050 $\pm 0.0212$ $\pm 0.48\%$	12.37 $\pm 0.13$ $\pm 1.02\%$	2.31	Statistical T Ratio	
Project = HLP Irradiation = OSUID09 J = 0.0015621 $\pm 0.0000070$ FCT-3 = 28.030 $\pm 0.003$ Ma			1.3407	Error Magnification		
					11	0.313 $\pm 0.006$

Appendix Table 8. Complete data from Noble Gas Spectrometry Laboratory analysis on sample HB17 (Swamp Creek Ash)





